INVESTIGATION INTO BIOMASS THERMAL TRANSFORMATIONS DURING HIGH TEMPERATURE FEEDING

A Thesis

by

RICK F. WANG

Submitted to the Office of Graduate and Professional Studies of
Texas A&M University
in partial fulfillment of the requirements for the degree of

MASTER OF SCIENCE

Chair of Committee,	Hong Liang
Committee Members,	Gwo-Ping Fang
	Bruce Tai
External Member,	Jun Qu
Head of Department,	Andreas Polycarpou

December 2020

Major Subject: Mechanical Engineering

ABSTRACT

Biomass, as a source of energy, has been increasing in popularity due to its widespread availability, low cost, and benefits to the environment. Especially in United States, biomass feedstock research and development has received additional funding in an effort maximize the potential of the vast forestlands and curb the country's dependence on conventional fossil fuels. However, variability in biomass feedstock properties, especially during high temperature processes, is the biggest obstacle in developing better models and technologies. The objective of this research is to investigate the thermal transformation of a biomass feedstock during a high temperature feeding process.

A high temperature screw feeder that experienced plugging issues was investigated. A 3D model and thermal simulation was used to develop the thermal profile of the screw feeder in the axial direction. Then, a thermal model was created to determine the temperature profile of the biomass in the radial direction at each flight section on the screw feeder. The predictions made by the model were then validated through characterization of the biomass deposit. Characterization was conducted using optical microscopy, scanning electron microscopy (SEM), and electron dispersive spectroscopy (EDS). Additionally, cross-sectional examination and nano-indentation were performed.

The locations where the model predicted the biomass would begin to burn was validated by the characterization results. There is also uneven heating in the biomass deposit according

to proximity from the tip and the contact interface with the screw feeder. Additionally, it was found that residence time has a significant influence on the heating of the biomass deposit. Plastic deformation discovered on the edges of the flight that have led to additional biomass accumulation as well as increased residence times.

The findings from this research are beneficial to the biomass feedstock industry. It will be useful in informing future screw feeder models and processes for screw feeders to improve efficiency and mitigate failures.

DEDICATION

This is dedicated to my family and friends who have supported me throughout this journey.

ACKNOWLEDGEMENTS

I would like to thank Dr. Liang, my committee chair, for guiding me and encouraging me throughout my graduate school experience. I would also like to thank Dr. Qu, for the research direction and invaluable learning experience at ORNL, and my committee members, Dr. Fang and Dr. Tai for their guidance and support in this research.

Additionally, I would like to thank everyone that I've met and interacted with along this journey, especially Dr. Kyungjun Lee and the members of the Surface Science Group for their help and constructive criticism.

I am also grateful for all the members of the Department of Mechanical Engineering staff and faculty at Texas A&M University.

Finally, I would like to show appreciation to my family for their unwavering support, love, and sacrifices for me to pursue my dreams.

CONTRIBUTORS AND FUNDING SOURCES

Contributors

This work is supervised by a thesis committee consisting of Dr. Liang and Dr. Tai of the Department of Mechanical Engineering, Dr. Fang of the Department of Engineering Technology and Industrial Distribution, and Dr. Qu at Oak Ridge National Laboratory.

Sample preparation and polishing was performed by Tom Geer at Oak Ridge National Laboratory. Nano-indentation was conducted by Alexis Betancourt at Oak Ridge National Laboratory.

All other work conducted for the thesis was completed by the student independently.

Funding Sources

This research was supported in part by an appointment to the Oak Ridge National Laboratory HERE Program, sponsored by the U.S. Department of Energy and administered by the Oak Ridge Institute for Science and Education.

NOMENCLATURE

Acronyms

CFD	Computational fluid dynamics
DOE	U.S. Department of Energy
EDX	Energy-dispersive X-ray spectroscopy
FTIR	Transform infra-red spectroscopy
INL	Idaho National Laboratory
NREL	National Renewable Energy Laboratory
ORNL	Oak Ridge National Laboratory
RS	Raman spectroscopy
SEM	Scanning electron microscope
SS	Stainless steel
TGA	Thermogravimetric analysis
TOF-SIMS	Time-of-flight secondary ion mass spectrometry
USDA	U.S. Department of Agriculture

Symbols

b	Contact area half-width

E	Elastic modulus
T	Temperature
Q	Thermal energy
$\dot{Q}$	Rate of heat transfer
K	Thermal conductivity
R	Thermal resistivity

TABLE OF CONTENTS

Page

LIST OF FIGURES

Page

LIST OF TABLES

Page

CHAPTER I

INTRODUCTION

This chapter provides the reader the necessary background information to develop a comprehensive understanding on the undertaken research. It gives an overview on biomass as an energy source. The pros and cons of bioenergy is covered as well as the different types of biomass and processes involved in the conversion to usable energy. The importance of the biomass feedstock to the renewable energy sector in the U.S. is also discussed. Following this is a review on screw feeders that examines general characteristics, working principles, and usage in the biomass feedstock industry. Finally, variability in biomass feedstock properties is investigated. As a result, its detrimental effect on feeder performance is realized and limitations in current models are identified.

1.1 Biomass as an energy source

1.1.1 Definition of biomass

Biomass, as a source of energy, is a plant-based material that is both organic and renewable [1]. The energy that can be harvested from plants comes from the absorbed solar energy through photosynthesis. In photosynthesis, radiant energy from the sun is used to convert water and carbon dioxide into oxygen and glucose. Biomass is produced from the carbon that the plant takes in from the carbon dioxide in the atmosphere.

Aside from the sun, biomass is the oldest source of energy used by humans. For thousands of years, humans have been using the energy derived from biomass through direct combustion for things such as cooking and heating. In the eighteenth century, the role of biomass expanded to provide heat, steam, and power for industrial processes [2]. In today's modern era, its implementation as a source of fuel energy has significantly expanded due the ever increasing global demand for energy, the rapid depletion of fossil fuel resources, and the disastrous effects of climate change caused from the carbon dioxide emissions of conventional fossil fuel processes. As a result, this has spurred both scientific and business sectors to develop new technologies or innovate and improve current systems and processes [3].

Biomass is advantageous to other forms of renewable energy for a number of reasons. It is considered as a widely available source of renewable energy that is both low cost and environmentally beneficial. Plants, as a carrier for the chemical energy converted from solar radiation, have great stability and capacity in energy storage. They can be harvested from a multitude of sources including agricultural lands, forests, and municipal waste. It is also extremely versatile and can utilized as a solid, liquid, or gas [4]. Additionally, biomass has the capability to assist global efforts in achieving zero emissions and sustainable development. Nevertheless, there are some disadvantages associated with biomass usage. Biomass resources are generally low in energy density, sensitive to season changes, and widely scattered at dispersed sites. Because of this, transportation is costly, and the technology required to efficiently produce useful energy is expensive. However, the

potential benefits outweigh the negatives and these obstacles can be overcome with improving technologies [5].

1.1.2 Types of biomass

As stated previously, biomass is extremely versatile and available from a wide range of sources. The five main types of biomass that are used for energy production, depicted in Figure 1, include woody biomass, agricultural biomass, solid waste, landfill gas, and alcohol fuels. These come from a variety of sources including wood and wood processing wastes, agricultural crops and wastes, municipal solid waste, and animal manure [6].

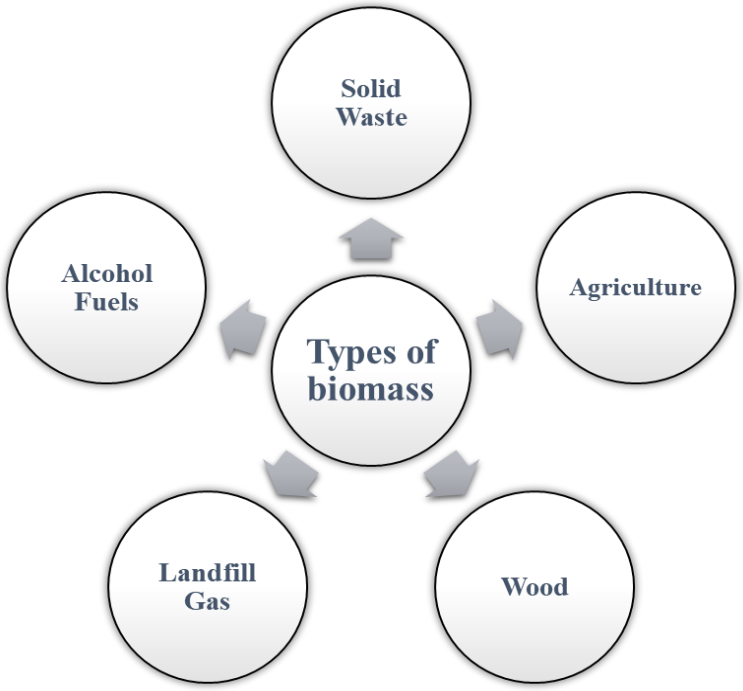

Figure 1. Types of biomass used for energy

Biomass feedstocks are materials that are harvested for the sole purpose of energy conversion. They can be separated into three main categories: primary, secondary and tertiary. Primary feedstocks are harvested and directly converted into bioenergy. Some examples of these are corn, vegetable oil, and recycled fats and grease. The waste from processing primary feedstocks are considered secondary feedstocks. These include agricultural residue, forest residue, urban woody waste, and landfills. Tertiary feedstocks, usually from construction and demolition sites, are derived from post-consumer waste [7,8].

1.1.3 Biomass conversion

After harvest, the biomass must undergo preprocessing before it can be converted to fuel. The purpose of preprocessing is to control variability in the physical and chemical properties of the feedstock in order to improve prediction models and maximize conversion efficiency. The two stages of preprocessing that all biomass feedstock go through are size reduction and drying, which controls particle size distribution and moisture content. Once preprocessing is complete, the feedstock moves to different conversion processes [9].

There are three categories of decomposition used in biomass feedstock conversion: thermochemical, biochemical, and chemical. The one most relevant to this research is thermochemical conversion. Thermochemical conversion uses thermal energy to convert the biomass into useful energy, usually in the form of electricity or heat. The two processes used in thermochemical conversions are gasification and pyrolysis, differentiating by the presence

or absence of oxygen during the process. Gasification takes place in the presence of oxygen and uses fixed bed and fluidized bed technologies. Pyrolysis takes place in the absence of oxygen and can be classified as slow or fast pyrolysis [10]. Figure 2 depicts the stages involved for a typical thermochemical conversion process.

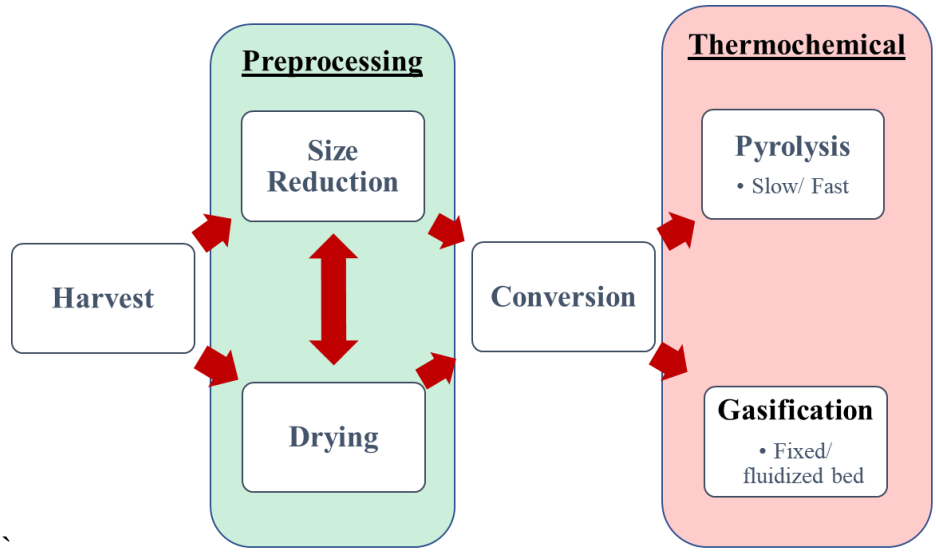

Figure 2. Process flow diagram for thermochemical conversion

1.1.4 Biomass feedstock industry in the U.S.

In 2019, the U.S. primary energy consumption was estimated to be a total of 100.2 quadrillion Btu. As shown in Figure 3, out of that total, 11.4% of energy was supplied by renewable sources. The renewable energy industry is projected to only increase as global crude oil prices rise, and the costs of renewable energy technologies drop [11-13].

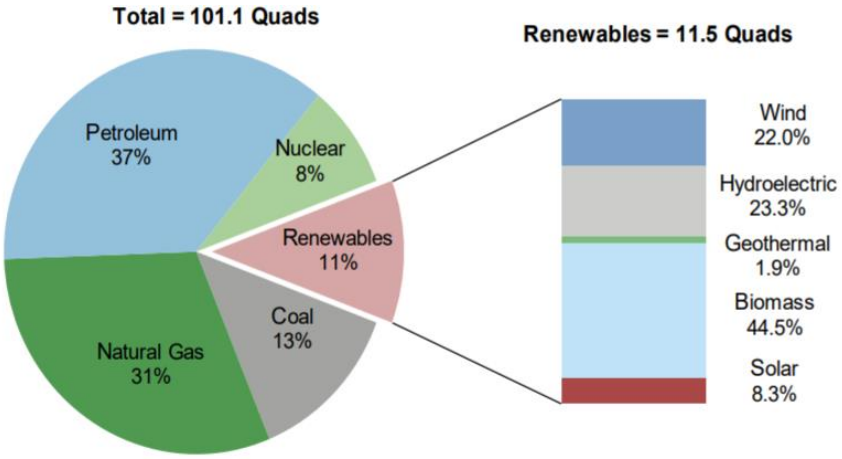

Figure 3. Breakdown of energy consumption in the U.S. [14]

The bioenergy industry is the largest portion of the renewable energy generated by the U.S. at 44.5%. The plot in Figure 4 tracks the consumption of renewable energy sources starting from 1950. Biomass as a major source of energy has been steadily increasing since 1975. Starting in the early 2000's, it became the leading source of renewable energy. This is partly due to the fact that biomass became recognized as a storable, substitutive, and abundant carbon neutral material [1].

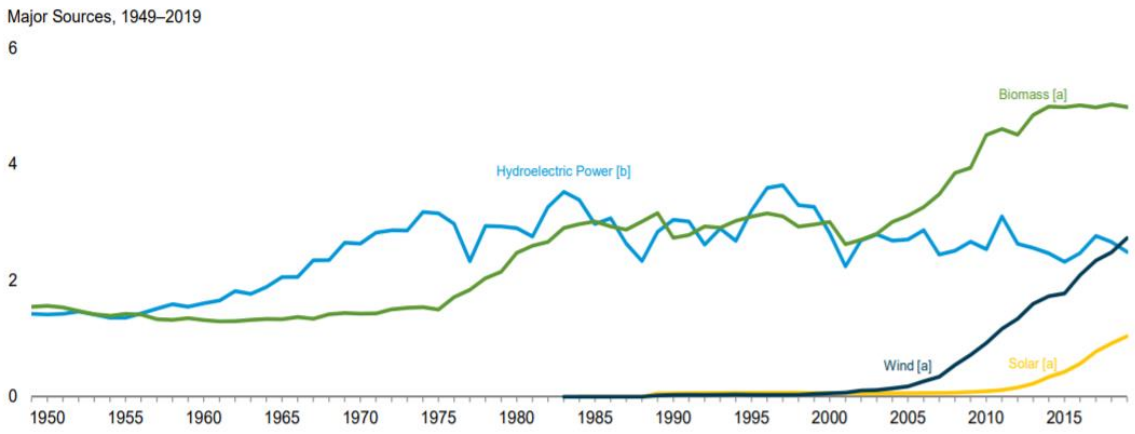

Figure 4. Renewable energy consumption (quadrillion Btu) [15]

In the U.S, the main applications for biomass are in transportation and electricity generation. As per of the Advance Energy Initiative, the U.S. Department of Energy (DOE) and the U.S. Department of Agriculture (USDA) are committed to replacing 30% of the total U.S. petroleum consumption with biofuels by 2030 [16]. This has led to increased funding for biomass feedstock research and development. Feasibility studies have estimated that 1 billion dry tons of biomass feedstock will be needed per year to accomplish this goal. In a survey of forest and agricultural lands, it was found that the U.S. has the potential to produce 368 million dry tons of forest resources and 998 million dry tons of agricultural resources, combining for a total of 1.366 billion dry tons per year, exceeding the estimated requirement. Particularly in the U.S, forest biomass has garnered a lot of interest due its large-scale availability. One-third, or 749 million acres, of the country's land mass is covered by forestland. About two-thirds, or 504 million acres, is considered harvestable [17].

1.2 Screw feeder

1.2.1 Definition

A screw feeder is a type of conveying system that is used to transport powder and granular materials. Although there are huge variations in both size and shape, the general design and operating principles remain the same. A typical screw feeder system, shown in Figure 5, consists of a trough or tube that encases a rotating screw. There are usually two openings, located on opposite ends, for the feed material to enter and exit the system. At the inlet, material is fed into the screw feeder by a hopper. The rotating screw within transports a continuous plug of materials to the outlet. The clearance between the screw and the housing is tight to prevent the backwards flow of materials. The system is usually powered by a motor. The power output from the motor is transmitted through a gear box and translates into rotational energy to turn the screw [18,19].

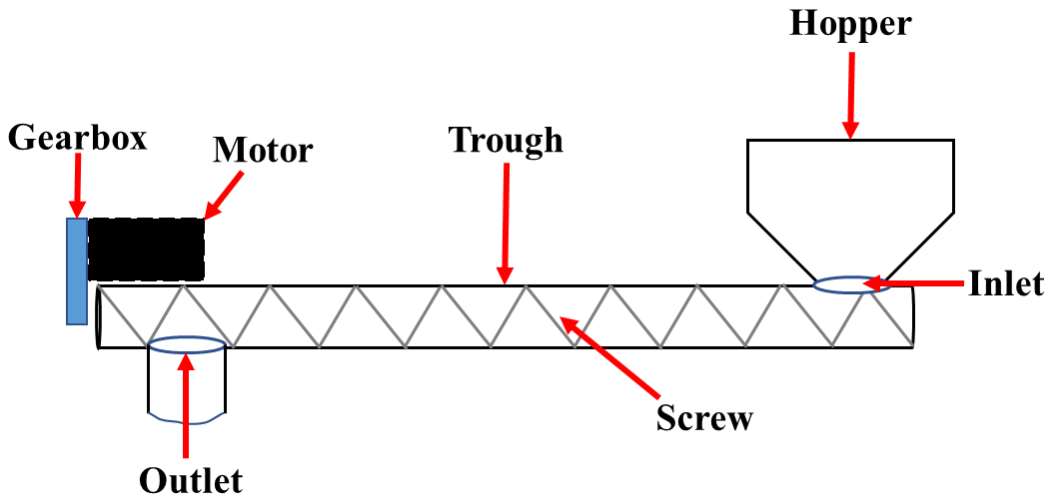

Figure 5. Typical design of a screw feeder system

1.2.2 Working principles

The main physical characteristics of a screw feeder system are shown a diagram in Figure 6 below. The driving side of the flight pushes material in the direction of feeding. The trailing side of the flight is the side facing opposite of the feeding direction. Some other important features to note that are relevant in this research are length, pitch, flight, flight outer diameter, and shaft diameter.

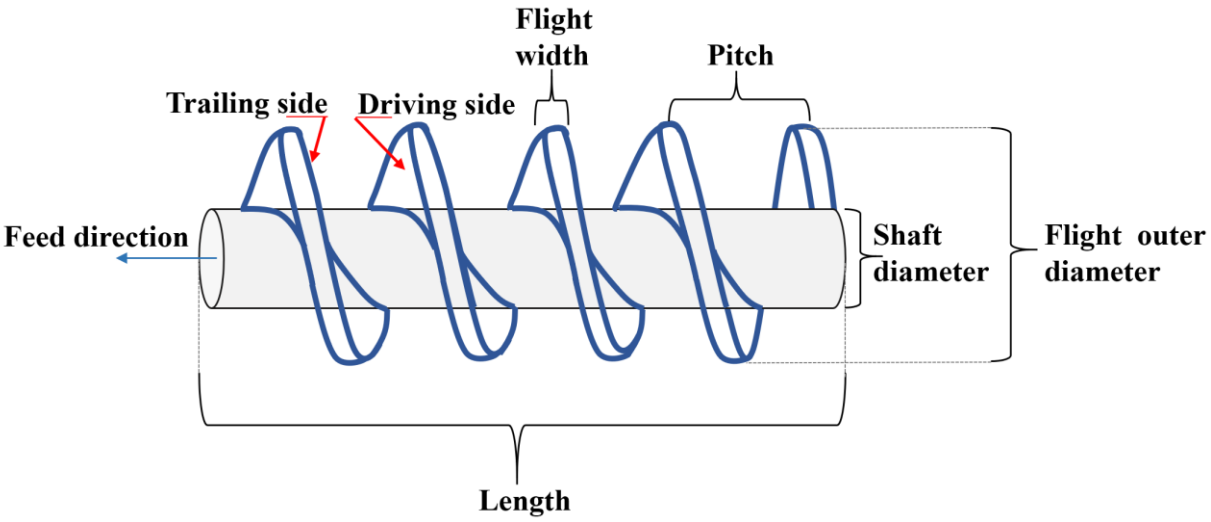

Figure 6. Physical characteristics of a screw feeder

The feed rate, or the rate the material moves through the feeder, is dependent on these physical characteristics. In ideal conditions, this rate is directly proportional to the rotational speed of the screw, making it easy quantify the volume of material passing through the system [19]. During feeding, the feed particles following a helical path as it is pushed by the

driving surface of the flight. The time it takes for a particle to travel from the inlet to outlet of the feeder is known as the residence time. The torque required to move the material can be also be calculated. This is determined by the forces acting on the boundaries surrounding the material within a flight section [20].

1.2.3 Applications in the biomass feedstock industry

In the biomass feedstock industry, screw feeders play a crucial role in energy conversion processes. Screw feeder systems are widely used for its capability to continuously feed material at a steady and controllable rate. Additionally, their flexibility in terms of feed material compatibility and sizing makes them suitable for a variety of applications. Generally, screw feeders are used to transport the biomass feedstock throughout the different stages of processing. However, there are also specialized screw feeders that are designed to feed biomass directly into pressurized reactors [21].

The modelling of screw feeder systems is a leading area of research in the development of new screw feeder technologies. Modelling attempts in recent studies have used discrete element method, multivariate analysis using principal component analysis, and partial least square regression to predict feeder performance based on material properties [22,23]. Other studies have been conducted on screw feeder parameters, such as geometry, rate, speed, and torque and the effect of those on feeding performance [24-26]. Advancements in screw feeder technology can also be attributed to the rapid growth and breakthroughs made in computational modelling. These models have superior computing capacity and are able to

process large data sets and generate more comprehensive simulations. These simulations are then used as tools to predict and improve screw feeder performance. Using this information, designs are optimized to achieve better process stability, reliability, and feed rate accuracy [23].

1.3 Feedstock variability

1.3.1 Effect on screw feeders

Despite all these developments, all modern screw feeder technologies suffer from the prevailing issue of variability in biomass feedstocks. The unpredictability in both the physical and chemical properties of biomass adversely affects almost all aspects of current screw feeder systems and has a negative impact on the overall conversion process. Size distribution, particle shape, moisture content, bulk/particle density, compressibility, contaminants, and flowability have all been identified as properties detrimental to screw feeder performance as well as modelling efforts [27].

Plugging or blockage is the most common type of failure experienced by screw feeders [28]. This is caused by material build-up on the screw that worsens as it is compacted as the screw feeder continues to operate, causing feed rate fluctuations and seizure. Mechanical wear and corrosion on the surface of the screw further accelerates this issue [27]. In addition to plugging, there have also been cases where screw feeders fail due to overloading. In one case, when a feeder was plugged, the motor powering the system continued to operate and

drive the screw. This resulted in excessive torsional stress on the screw shaft, producing cracks. Poorly designed systems are also subject to bending stress failures. In another case, the shaft of the screw was not adequately supported and experienced bending stress due to the weight of the assembly. As a consequence, cyclic stress overloaded the screw and caused fatigue failure [29]. If these failures were to materialize when the screw feeder is in operation, the results can be catastrophic, leading to equipment damaged, increase downtime, and an overall negative impact on the economics of biomass feedstock processing [30].

1.3.2 High temperature conversion processes

When high pressure and/or high temperature is introduced into the conversion process, variability in biomass properties is compounded as the biomass decomposes into solid char and ash, non-condensable gases, and multiple liquid phases [31]. Char directly impacts the performance of the conversion process and has been deemed a critical area of research. Extensive research has been undertaken to characterize biomass at elevated temperatures to develop a better understanding its properties to improve current models and processes. Since there are so many different types of biomass and conversion processes, research has been done in developing a new classification system to cover char structures based on biomass type, original lignocellulosic composition, and cell structure [32].

Characterization efforts investigate chars from different sources of biomass as well as at varying temperatures simulative of different conversion processes. A summary of various

characterization approaches is presented in Table 1. One study examined the yield, chemical composition, surface chemistry, structure, morphology, and reactivity of beech wood chars prepared at temperatures ranging from 500-1400˚C using scanning electron microscope (SEM), energy-dispersive X-ray spectroscopy (EDX), transform infra-red spectroscopy (FTIR), Raman Spectroscopy (RS), and thermogravimetric analysis (TGA) [33]. Pore structure properties of pine chars have also been examined to study adsorption capacity [34]. The properties from char produced from gasification of deal-coholised marc of grape was characterized to improve current gasification processes [35]. Another study researched the buildup of olivine ash to better understand its influence on fluidized bed gasification processes [36]. Multiple studies have been done studying char residue for pyrolysis reactions. One such study produced char at 1000˚C then used SEM and oil immersion microscopy to determine degree of deformation, internal particle structure, and wall thickness [37]. Cellulose and lignocellulosic biomass were pyrolyzed under atmospheric pressure at 700˚C for 4 hours then investigated using time-of-flight secondary ion mass spectrometry (TOF-SIMS), IR spectroscopy, and SEM to study the alteration and composition of the material's surface [38]. The porosity, particle density, bulk density, point of zero charge, surface pH, surface charges, water-absorption capacity, and surface area of mustard plant, groundnut plant, cotton plant, wheat plant, pigeon peas, and groundnut shell pyrolyzed at 650˚C have also been studied using X-ray fluorescence, proximate and ultimate analyses, SEM , and FTIR [39]. In addition to post-reaction characterization, real-time microscopic analysis has been conducted. Poplar wood samples were studied during pyrolysis revealing a pattern of tissue and macropore expansion and collapse [40].

Table 1. Comparison in different characterization approaches

Material	Techniques	Properties characterized	Reference
Beech wood char (500-1400˚C)	SEM, EDX, FTIR, RS, TGA	Yield, chemical composition, surface chemistry, structure, morphology, reactivity	[33]
Deal-coholised marc of grape	TGA, calorimeter, SEM, FTIR	Structural, thermochemical, and compositional properties	[35]
Olivine ash	XRD, SEM, EDS, X-ray microtomography, FTIR, RS	Morphological changes of particle surface of ash layer	[36]
Char (1000 ˚C)	SEM, oil immersion microscopy	Deformation, internal particle structure, wall thickness	[37]
Cellulose & lignocellulosic (700 ˚C)	TOF-SIMS, IR spectroscopy, SEM	Surface composition and structure	[38]
Mustard plant, groundnut plant, cotton plant, wheat plant, pigeon peas, groundnut shell (650 ˚C)	X-ray fluorescence, SEM, FTIR	Porosity, particle/bulk density, point of zero charge, surface pH, surface charge, water-absorption capacity, BET surface area	[39]
Poplar wood	Real-time microscopic analysis	Pattern of macropore expansion/collapse	[40]

One method proposed to improve conversion efficiency is pretreatment. To evaluate various pretreatment technologies, characterization is again used to examine the biomass char post-conversion. One study reviewed and summarized the effectiveness of various thermal and chemical pretreatment processes [31]. Additionally, the effectiveness of one pretreatment technology on switchgrass was investigated through examining the structural impacts on plant tissue, cellular, and call wall levels [41]. A pretreatment method using ammonia and organosolv was also studied using TOF-SIMS to find a correlation between surface cellulose and glucose release after hydrolysis [42].

Models have been developed with the goal creating more accurate predictions on biomass char properties and output during these high temperature processes. Table 2 summarizes the different approaches used to model biomass behavior. One such study developed a char oxidation model based on the characterization of char reactivity to oxygen and surface area. This model investigated to effects of surface oxides and surface area evolution[43]. The gasification of biomass has been modelled with a variety of approaches. One such approach is by performing numerical simulation using the discrete phase model for biomass particles. This model studied the influence of mass/mole fraction, concentration, and hydrodynamics during gasification [44]. Also, a mathematical model based on the traditional spherical biomass particle model was developed to predict carbon conversion during CO_2 gasification of biomass [45]. Similarly, a kinetic model was developed to predict results for a flow reactor performing CO_2 gasification of biomass [46]. Another model employed realistic morphology and explicit microstructure to improve on the traditional simplified spherical biomass

particle model to generate more accurate finite element simulations on particle to particle heat and mass transfer [47]. The single particle model has been used to model combustion behavior of biomass. One such study applied it to generate a CFD model to study biomass high-temperature rapid combustion [48]. In another study, the model was applied with high-speed and high-resolution imaging to observe the combustion behavior or differing biomass particles [49]. More recently, one study found success using a machine learning-based regression which outperformed traditional models when predicting biomass gasification results [50].

Table 2. Summary of various approaches to model biomass

Model	Topic	Approach	Reference
Char oxidation model	Effects of surface oxides and surface area evolution	Based on the characterization of char reactivity to oxygen	[43]
Numerical simulation	Influence of mass/mole fraction, concentration, and hydrodynamics during gasification	Discrete particle model	[44]
Mathematical model	Carbon conversion during CO_2 gasification of biomass	Traditional spherical biomass particle model	[45]

Table 2 Continued

Steady state kinetic model	Predict results for a flow reactor performing CO_2 gasification of biomass	Based on plug flow analogy for heat and mass balance	[46]
Biomass Particle Models with Realistic Morphology	Generate more accurate finite element simulations on particle to particle heat and mass transfer	Realistic morphology and explicit microstructure	[47]
Single particle model	Biomass high-temperature rapid combustion	CFD model	[48]
Single particle model	Combustion behavior or differing biomass particles	High-speed and high-resolution imaging	[49]
Predictive modelling	Predict biomass gasification results	Machine learning-based regression	[50]

In past studies, the focus has been on the characterization and modelling of biomass feedstocks for high temperature processes. Characterization is often done post-conversion when the biomass has decomposed into char. Modelling efforts either improve on current particle models or are developed to predict char behavior post-conversion. There exists a gap in knowledge on how biomass behaves in the pre-conversion stage. When the feedstock is fed into a high-temperature reactor via screw feeder, the biomass will undergo a large temperature gradient due to the reactor temperature at the outlet and typically room temperature at the inlet. This is known as high-temperature feeding. Because of this

temperature gradient, the biomass will begin thermal decomposition, which will lead to failures before the conversion process can take place. This research will focus on the pre-conversion process and will investigate the thermal transformation of biomass during high temperature feeding .

1.4 Summary

Biomass is defined as a plant-based material that can be harvested to produce energy. As the world shifts away from fossil fuel consumption, biomass emerged as the leading source of renewable energy. It is advantageous over other forms of renewable energy for its widespread availability, low cost, and benefits to the environment. Biomass feedstock comes in five forms: woody biomass, agricultural biomass, solid waste, landfill gas, and alcohol fuels. After harvest, the feedstock undergoes preprocessing prior to conversion. Preprocessing serves to control feedstock variability to optimize conversion efficiency. The biomass feedstock is then converted to usable energy through thermochemical, chemical, or biochemical methods. The vast forestlands in the U.S. has led to increased funding for biomass feedstock research and development in an effort to maximize the potential of the widespread availability of woody biomass to replace the country's dependence on fossil fuels.

Screw feeders are widely used in the biomass feedstock industry and offer one area of optimization to further improve the performance of conversion processes. They are favorable due to their continuous and steady feeding characteristics and can be modified to fit a variety

of applications. However, progress is hampered by the issue of variability in physical and chemical properties of biomass. Current models are not able to account for the unpredictability of biomass properties, especially due to high temperatures. This research will investigate biomass thermal transformations during high-temperature feeding.

CHAPTER II

MOTIVATION AND OBJECTIVES

As discussed in the previous chapter, the biomass feedstock industry is the biggest source of renewable energy in the U.S. and screw feeders are a critical component in the conversion process. Current research focuses on the post-conversion characterization and modelling of biomass feedstock after it decomposes to char. However, during high temperature feeding, the feedstock experiences across large thermal gradients along the screw feeder and the thermal decomposition of biomass is accelerated. Coupled with the high compressive forces that occur if plugging were to happen, the result is catastrophic failure, leading to extensive equipment damage, increased downtime, and an overall negative impact on the economics of biomass feedstock processing.

My research aims to fill the gap that exists in regard to biomass feedstock behavior during high temperature feeding and provide insight on how biomass transforms when subjected to large thermal gradients. This research will investigate the evolution of biomass deposit on a high temperature plug screw feeder and assess the thermal profile of the biomass using digital computation methods.

The objectives of my research are as follows:

1. Develop a thermal model of the system as a tool to validate current and future experimental data
2. Perform characterization to understand the evolution of the biomass deposit across thermal gradients
3. Identify the mechanisms causing the biomass agglomeration and consequently, screw feeder plugging

These objectives will be achieved by following the approach outlined in the flow chart in Figure 7. First, a model will be created for the screw feeder system that is being investigated. This model will be used to generate thermal profiles in both the axial and radial directions of the system. The results from this model will be used to investigate the heat transfer that is occurring between the biomass deposit and screw feeder and provide insight on the temperature experienced by the biomass during the feeding process.

Next, characterization will be performed on the biomass deposit to validate the results obtained from the thermal model. Characterization will begin with surface morphology examination to study the difference in microstructure of the deposit at different sections on the screw feeder. Then, the composition and hardness of the biomass at each section on the screw feeder will be analyzed. The purpose of this characterization approach is to gain an understanding of how the structure and composition of the biomass deposit transforms as it is subjected to an increasing temperature gradient.

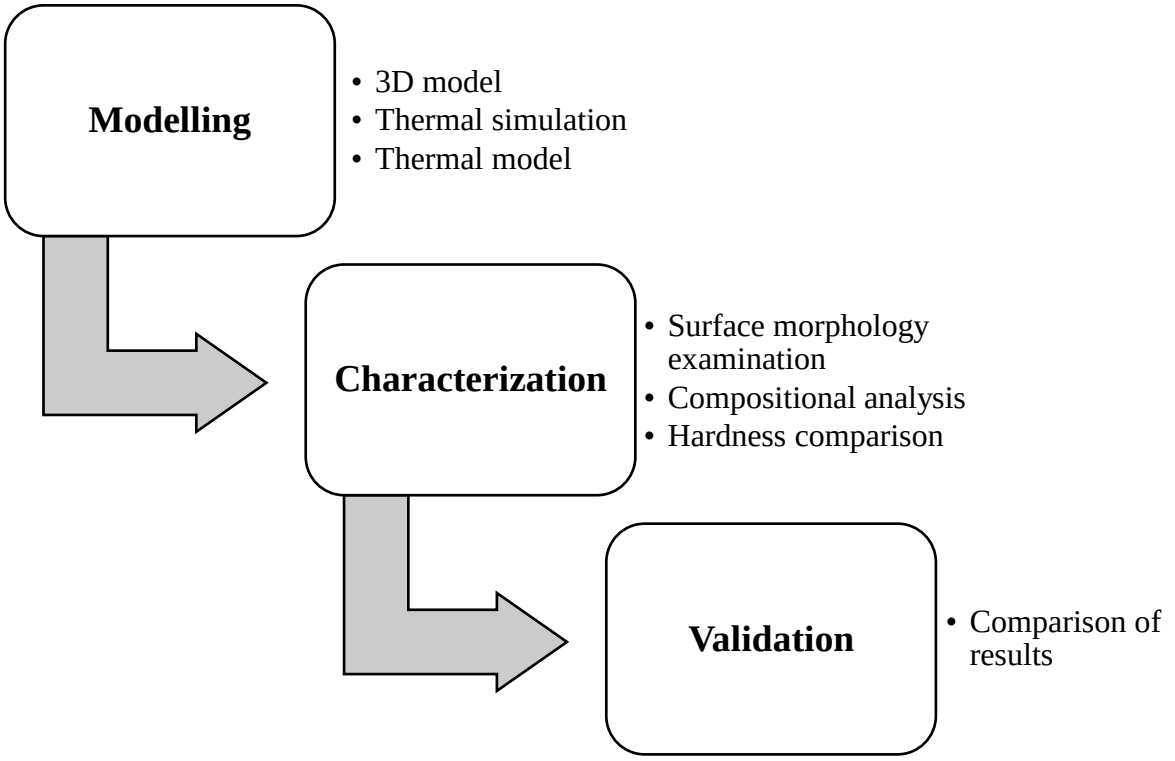

Figure 7. Research flowchart

The findings from this study will be used to inform future designs for screw feeders and mitigate plugging issues during high temperature feeding. This will be beneficial to the biomass feedstock industry as the country moves away from conventional fossil fuels and shifts towards renewable energy. Thus, increasing the demand for more efficient and lower cost processing methods to maximize the potential of biomass and biofuels as sources of energy.

CHAPTER III

MATERIALS AND METHODS

This chapter discusses the materials and methods used for characterization of the biomass deposit in this research. The first section includes the biomass feedstock materials and processes involved in the particular screw feeder system that is being investigated. A 3D model of the system was created and thermal simulations were performed using SolidWorks 2020. Then, the different characterization methods used in this research are explained. Surface morphology, chemical composition, and hardness of the biomass deposit were characterized using optical microscopy, scanning electron microscopy (SEM), electron dispersive spectroscopy (EDS), and nano-indentation.

3.1 Materials

The focus of this research is on a screw feeder that experienced plugging issues due to biomass agglomeration during high temperature feeding. This screw feeder was a part of a small-scale experiment at the National Renewable Energy Laboratory (NREL) that was used to transport preprocessed biomass into a pyrolysis reactor for energy conversion. This is known as the preconversion stage, as this screw feeder acts as an intermediate step, connecting the preprocessing and conversion stages. The screw feeder material is 304 stainless steel and the trough/housing that encases the screw is made of 316 stainless steel.

As seen in Figure 8, the first six flight sections of the screw feeder are where the most severe biomass agglomeration have occured. This accumulation towards the tip of the screw has resulted in stoppages leading to significant downtime in normal operations and in extreme cases, caused the screw to back itself out of the trough and housing, damaging the whole system. Therefore, these six sections have been identified as the primary area of interest on the screw feeder and will be the focus of this research. The tip is exposed to the pyrolysis reactor temperature of 500 ˚C, while the other end is at room temperature. The biomass feedstock enters the screw feeder at room temperature and is subjected to increasing temperatures as it travels towards the outlet where the temperature is the same as that of the pyrolysis reactor.

Figure 8. Screw feeder as received with severe biomass accumulation towards the tip

This particular screw feeder ran a 50/50 blend of pine and forest residue. The feedstock was harvested from loblolly pine trees in Screven County, GA and Edgefield County, SC. The trees were broken down to a nominal chip size of 2 in. and shipped to Idaho National Laboratory (INL) for further processing. The chips are then passed through another chipper fitted with a ¾ in. screen. After this, the feedstock is fed through a dryer and dried to 30% moisture. Then, the materials pass through a second stage grinder fitted with a ¼ in. screen

and dried again to 10% moisture [31]. Once this is completed, the feedstock is transported to NREL for experimentation. A diagram of these processes is presented in Figure 9.

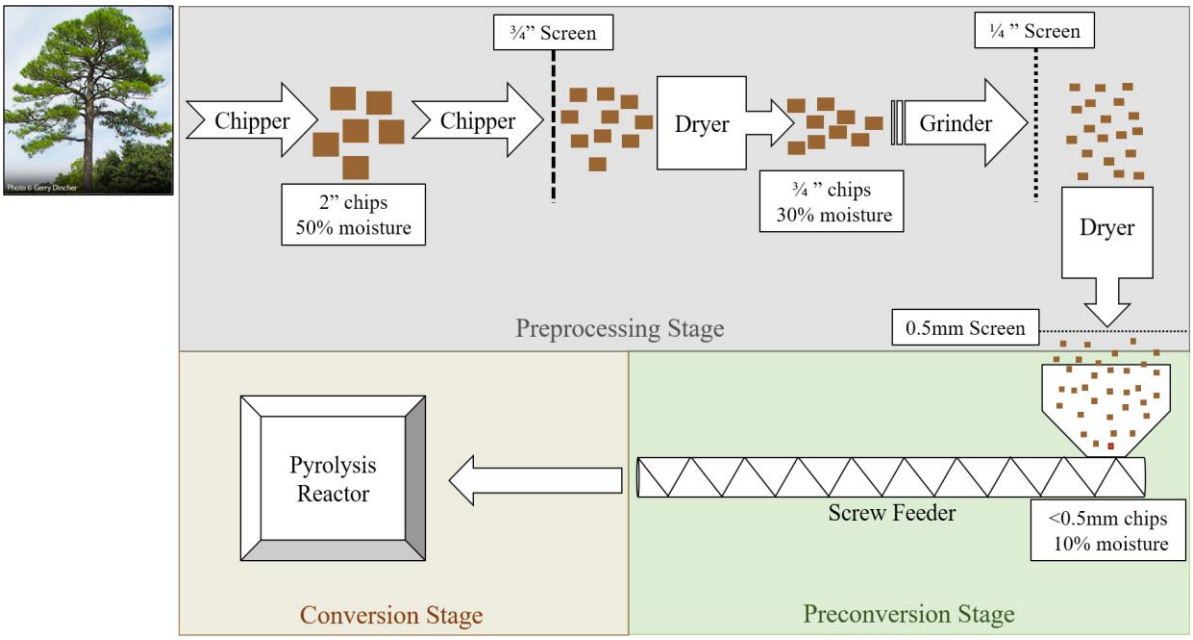

Figure 9. Process flow diagram of biomass feedstock from preprocessing to conversion stages

When the biomass reaches the preconversion stage, the chips have been downsized to particles of dimensions less than 0.5mm. The feedstock material, shown in Figure 10, is more representative of fine dust particles rather than wood chips at this point. Initial visual observations reveal that the biomass is extremely loose in structure. Individual particles easily detach and separate in areas where they are not tightly packed.

Figure 10. Biomass feedstock: 50/50 blend of pine and forest residue

3.2 Modelling

SolidWorks 2020 was used to generate a 3D model of the system. SolidWorks Simulation was used to perform thermal simulations. A thermal model of the system was built using Microsoft Excel to characterize the heat transfer from screw to biomass.

3.3 Characterization methods

3.3.1 Sample preparation

The first six flight sections of the screw feeder that are being investigated was sectioned into three segments, each containing two sections, by a dry cutting method intended to preserve the integrity of the biomass deposits on the surface of the screw. This method was successful as minimal biomass was lost during the process. After initial characterizaion was completed, the samples were then cross-sectionally cut in the axial direction, mounted in epoxy, and

polished for further examination. During this process, moderate amounts of biomass particles were loss in sections where the deposit was looser. However, a sufficient amount remained on the surface of the screw feeder for analysis.

3.3.2 Image processing

Optical microscope images and SEM images were processed and analyzed using ImageJ software. The software was used to set scale bars on all images and calculate parameters such as particle size and length.

3.3.3 Surface morphology and chemical composition

Surface morphology characterization began with optical microscope imaging. Images were taken using the Southern Micro Instruments optical microscope, shown in Figure 11 below, with PAXcam image capture software. Images were taken from low to high magnification up to x200.

Figure 11. Southern Micro Instruments Optical Microscope

SEM images of the surface were taken using the HITACHI S-4800 Field Emission Scanning Electron Microscope shown in Figure 12. SEM images were taken at magnifications of x50, x100, x300, and x1000. 10 kV was chosen as the optimal voltage as anything higher would charge the biomass and disrupt the image quality. Chemical composition analysis and elemental mapping of the biomass deposit were performed using AMETEK EDAX system.

Figure 12. HITACHI S-4800 Field Emission Scanning Electron Microscope

Figure 13. AMETEK EDAX EDS System

3.3.4 Hardness

Nano-indentation was used to obtain hardness measurements of the biomass at various locations on the screw feeder. Indents were conducted by the Hysitron TriboIndenter TI-900 using the high load transducer with a Berkovich diamond tip. The Berkovich diamond tip was calibrated using a standard fused silica sample. The indents were performed under

displacement control of 700-800nm for each indent, reaching depth for 5 seconds, holding for 2 seconds, then releasing to 0 displacement in 5 seconds.

CHAPTER IV

THERMAL SIMULATION AND MODELLING

This chapter covers the method used to model the screw feeder system and biomass and discusses the results obtained from the thermal analysis. The purpose of developing a thermal model of the system is to understand the heat transfer that the biomass experiences during high temperature feeding. This will provide insight on thermal profiles of the screw feeder and the biomass. From this, correlations can be made to inform future optimizations.

A SolidWorks model and thermal simulation are used to generate the axial temperature profile of the screw feeder. Then, the temperature profile of the biomass is developed in the radial direction. Hertzian contact theory and the three modes of heat transfer are be discussed. Finally, results from the model are presented and analyzed.

4.1 Hertzian contact

In classical contact mechanics, Hertzian contact theory forms the basis of all contact mechanics used today [32]. This theory refers to the contact area and stress that results from the elastic deformation between two elastic bodies when they come into contact. What was previously modelled as a point or line contact between rigid bodies, now becomes an area contact [33]. The solution for this theory is based on the following assumptions [34]:

1. The surfaces are continuous and nonconforming
2. The surfaces are frictionless
3. The strains related to the deformations are small
4. Each solid can be considered as an elastic half-space near the contact zone

Hertz first used this theory to analyze the contact between a rigid sphere and elastic half-space. This was then adapted to solve for a variety of contacts, such as: sphere on sphere, sphere in cup, cylinder on cylinder, and cylinder in inner cylinder.

In this study, cylinder on cylinder contact was used and adapted to represent the contact between the biomass and screw feeder. Two parallel cylinders in contact, shown in Figure 14, have a rectangular contact area with width of $2b$. The half-width of that contact area, b, can be found using Equation 1.

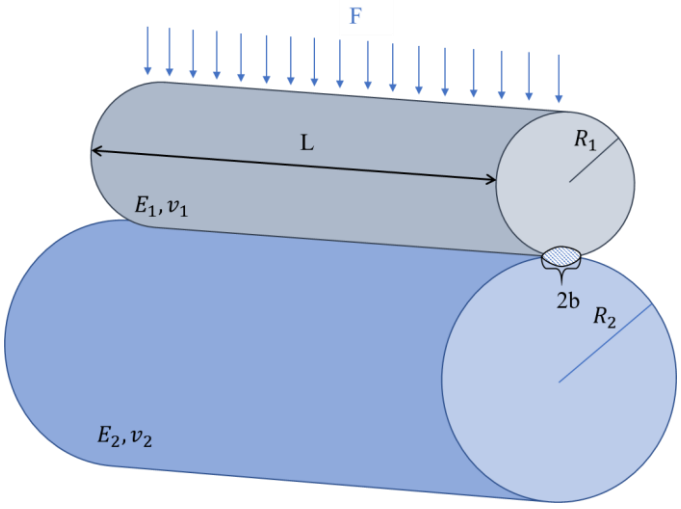

Figure 14. Cylinders in contact

$$b = \sqrt{\frac{4F\left(\frac{1-v_1^2}{E_1}+\frac{1-v_2^2}{E_2}\right)}{\pi L\left(\frac{1}{R_1}+\frac{1}{R_2}\right)}} \qquad (1)$$

Where, E_1 and E_2 are the elastic moduli for cylinders 1 and 2, v_1 and v_2 are the Poisson's ratio for cylinders 1 and 2, and L is the length of contact.

As stated previously, the biomass entering the screw feeder have been broken down to an optimal feed size of less than 0.5 mm and can be represented as a 0.3x0.3x0.4mm chip. Therefore, a more accurate representation of the contact between the chip and the screw feeder will be cylinder on flat. Equation 1 is adapted where the radius representing the biomass will become infinite since it is now a flat surface.

4.2 Heat transfer

4.2.1 Specific heat capacity

One method to measure the amount of thermal energy transferred to a material can be done using its specific heat capacity. Specific heat capacity, c_p, is a material property that defines the amount of energy required to raise the temperature of one unit mass of a substance by one degree [35]. When given a heat source, the temperature change can be calculated using Equation 2.

$$Q = mc_p\Delta T \qquad (2)$$

Where, Q is thermal energy, m is mass, c_p is specific heat, and ΔT is the difference in the initial and final temperature of the material.

4.2.2 Conduction

The tip of the screw at the outlet is exposed to the temperature of the pyrolysis reactor and by conduction, this heats up the rest of the screw. Conduction is the transfer of energy from higher energy particles to adjacent lower energy particles and can take place in solids, liquids, and gasses [35]. Fourier's law (Equation 3) states that the rate of conductive heat transfer is proportional to the temperature gradient through a layer of material. It takes into account the thermal conductivity of the material, contact area, and thickness.

$$\dot{Q}_{cond} = kA\frac{\Delta T}{\Delta x} \qquad (3)$$

Where, k is the thermal conductivity, A is the contact area normal to the direction of heat transfer, ΔT is the temperature difference across the material, and Δx is the thickness of the material.

Thermal conductivity is a material property that measures the rate of heat transfer through the material and is dependent on microstructure [36]. Thermal resistivity is the reciprocal of thermal conductivity and measures a material's ability to resist heat transfer. This is calculated using Equation 4.

$$R = \frac{x}{kA} \qquad (4)$$

Where, x is the material thickness, k is the thermal conductivity, and A is the contact area.

4.2.3 Convection

On the other end at the inlet, there is convection, where the surface of the screw is exposed to the environment at room temperature. Convection is the transfer of energy between a solid in a fluid medium [35]. The rate of heat transfer is dependent on the convective heat transfer coefficient, contact area, and temperature difference of the material surface and bulk fluid temperature. The convective heat transfer coefficient varies according to the type of convection and fluid medium. The rate of heat transfer is determined from Newton's law of cooling and is presented in Equation 5.

$$\dot{Q}_{conv} = hA(T_s - T_f) \qquad (5)$$

Where, h is the convective heat transfer coefficient, A is the contact area, T_s is the surface temperature of the material, and T_f is the temperature of the fluid.

4.2.4 Radiation

Preliminary calculations reveal that the biomass does not remain on the surface of the screw long enough for steady state conduction to occur. Therefore, thermal radiation is considered the main component of heat transfer from the screw feeder to biomass. Thermal radiation is the energy emitted by a body in the form of electromagnetic waves due to temperature [35]. Any body above absolute zero will emit thermal radiation. The Stefan-Boltzmann law measures the rate of radiative heat transfer assuming the surface is a blackbody. A blackbody is an idealized case where the surface is a perfect absorber and emitter since it can emit and absorb radiation at any frequency or angle of incidence. This means that a blackbody has the maximum rate of heat transfer. However, a real material has an emissivity property, which is a ratio ranging from 0 to 1, depending on its capability in emitting or absorbing radiation. This emissivity value approximates how close the surface is to a blackbody. The rate of radiative heat transfer of real materials is calculated using Equation 6.

$$\dot{Q}_{rad} = \varepsilon \sigma A T^4 \qquad (6)$$

Where, ε is emissivity, σ is the Stefan-Boltzmann constant ($5.67x10^{-8}\frac{W}{m^2K^4}$), A is the surface area, and T is the temperature of the body.

The intensity of the radiation emitted from a source will decrease over distance. This is known as the inverse square law, where the radiation from a source is inversely proportional to distance squared [37]. This relation is shown in Equation 7 and visualized in Figure 15.

$$Intensity \propto \frac{1}{d^2} \quad (7)$$

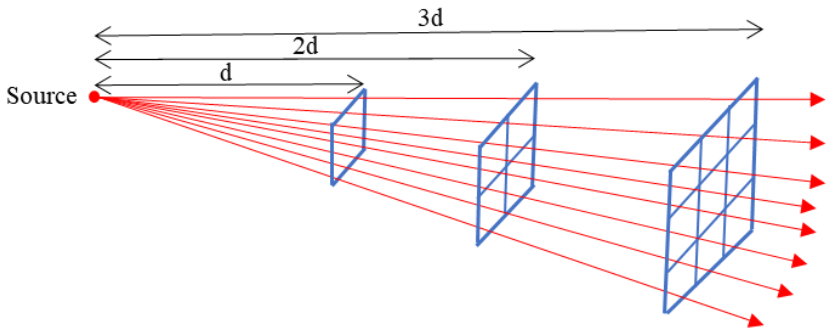

Figure 15. Inverse square law visualization

4.3 Thermal analysis of the screw feeder

4.3.1 3D modelling

A 3D model of the screw feeder and trough, shown in Figure 16, was created using Solidworks. In this model, the total length of the screw was taken at 12 inches with a pitch of 1 inch and outer diameter of 3/8 inch. The height of the flight is 0.079 inches (2 mm), giving a shaft diameter of 0.296 inches. This model generates a total of twelve sections for thermodynamic analysis. The trough is a tube with outer diameter of 0.625 inch and thickness of 0.065 inch.

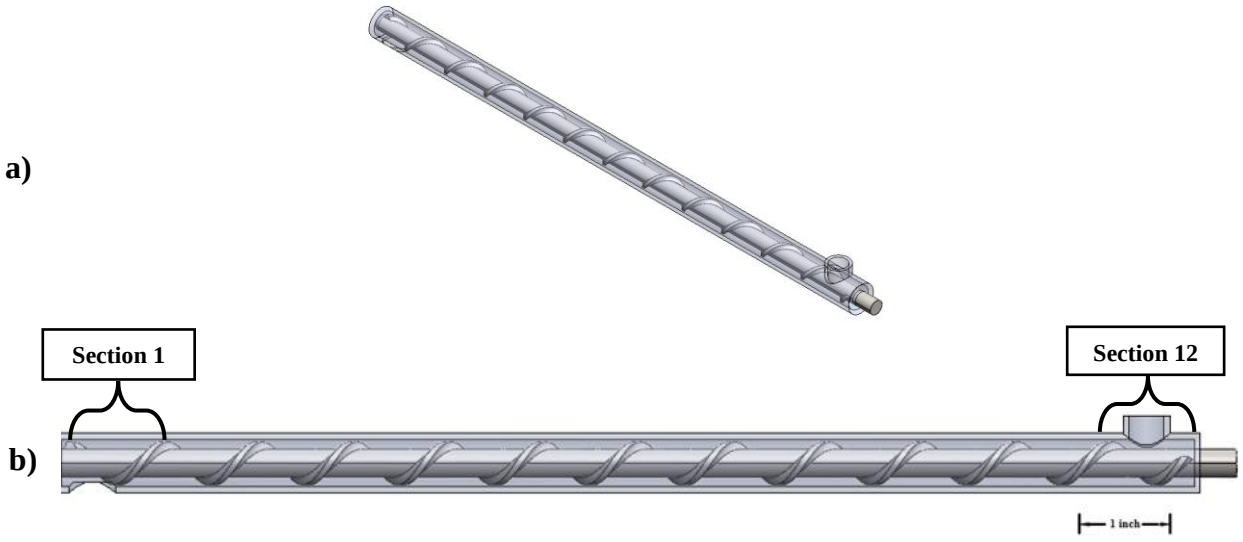

Figure 16. 3D model of screw feeder and trough: (a) isometric view (b) side view with tip and end sections labelled

4.3.2 Thermal simulation

It is known this screw feeder is part of the preconversion process, transporting preprocessed biomass into a pyrolysis reactor for high temperature conversion. The tip of the screw feeder is exposed to the pyrolysis temperature of the reactor, which is 500 ˚C. In the simulation, this temperature was applied at the tip of the screw feeder, as shown in Figure 17. By conduction, the rest of the screw is heated from this source.

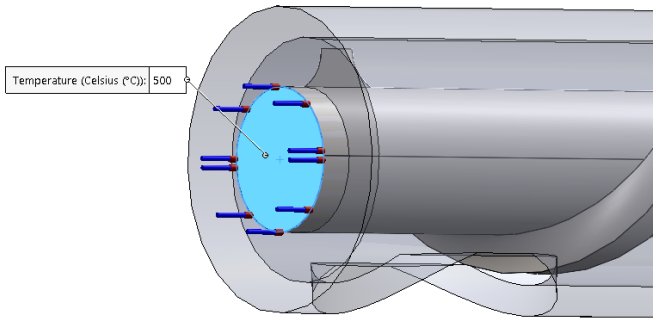

Figure 17. Surface where the 500 ˚C temperature source was applied (in blue)

The other end of the screw is exposed to room temperature. This was modelled as convective heat transfer at an ambient temperature of 25˚C, as shown in Figure 18. The convective heat transfer coefficient was taken at 50 W/m^2K, assuming free convection in air.

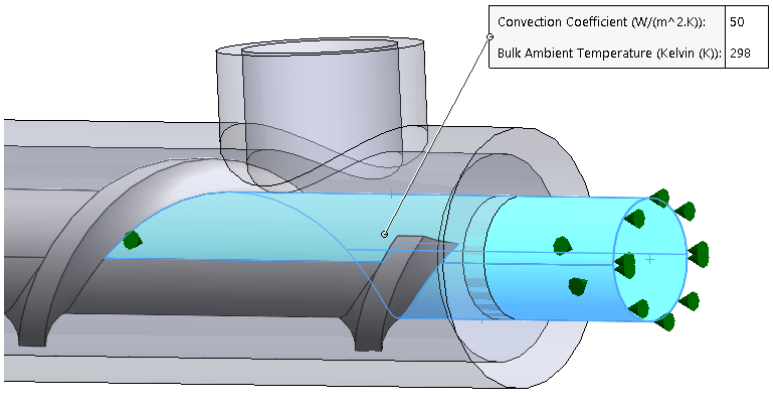

Figure 18. Surface where the screw is exposed to free air convection (in blue)

The interface of the screw feeder and the trough (highlighted in purple in Figure 19) was modelled as a thermal resistance. The thermal resistance was calculated to be 8.688 K/W and took into account the thermal conductivity of 316 SS and the contact area between the two components.

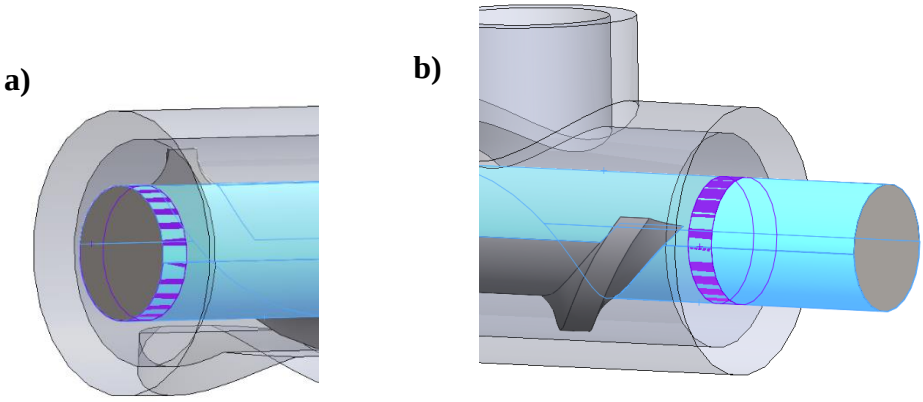

Figure 19. Thermal resistance contact interface at (a) tip and (b) end

The resulting axial temperature profile obtained from this simulation is shown in Figure 20. A plot of the result is presented in Figure 21. From the figure, the screw feeder experiences a maximum temperature of 500˚C at the tip of Section 1 and a minimum 99.8˚C at the end of Section 12. It is known that the ignition temperature of wood is around 300˚C [38]. The screw feeder is at this temperature at Section 6, about 5.75 inches from the tip. The temperature for each section was taken in middle, which is also the average temperature of the section because the temperature decreases linearly by conduction through the screw feeder. Only in Section 12 is where this rate is not linear due to the effect of convection.. These temperatures form the basis of the calculations for the thermal profile of the biomass in the radial direction that will be discussed in the next section.

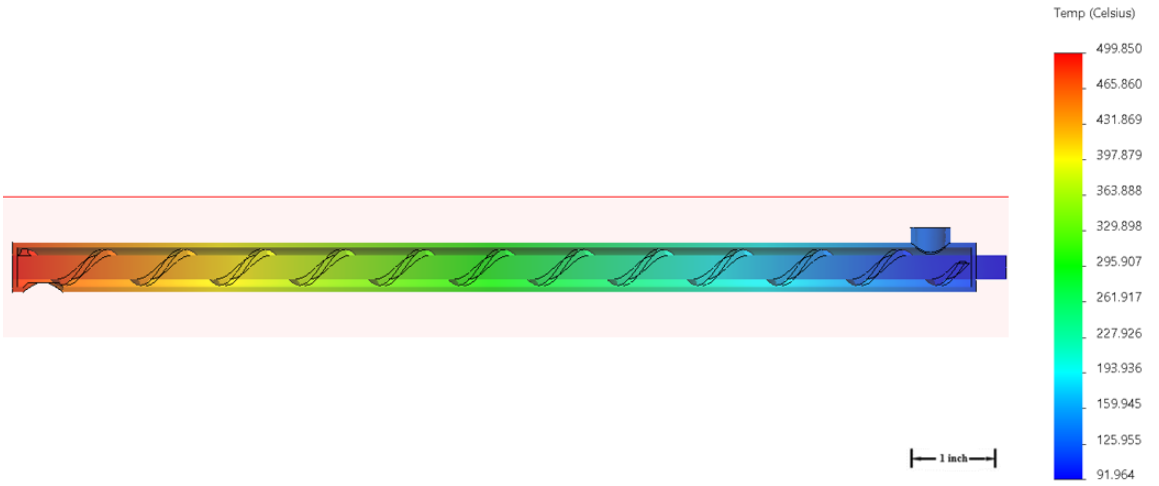

Figure 20. Axial temperature profile of screw feeder

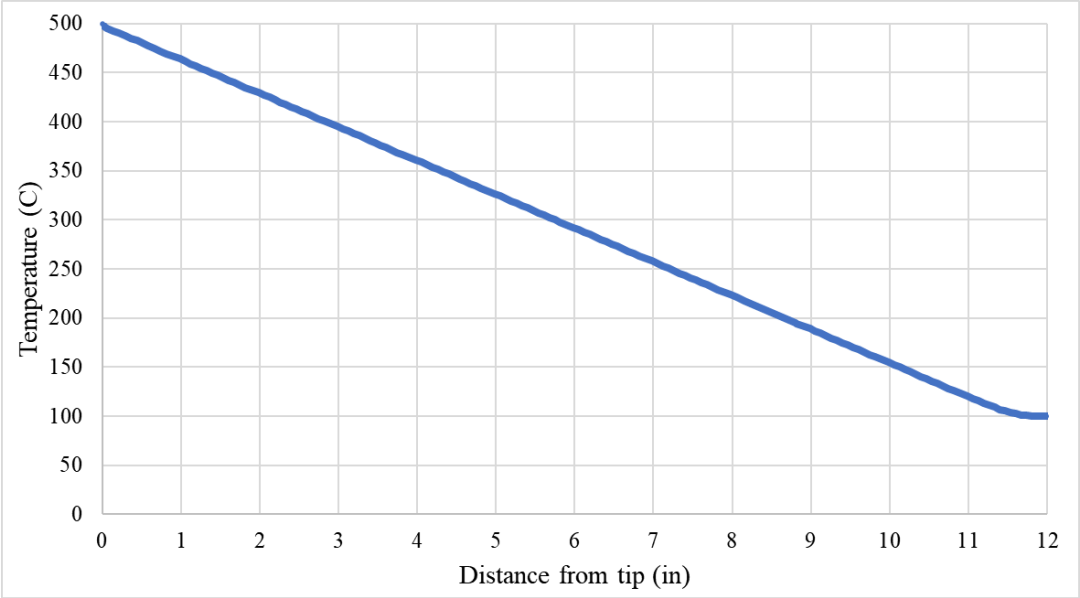

Figure 21. Plot of temperature change versus distance from the tip

4.4 Thermal modelling

4.4.1 Assumptions

In this model, the biomass is represented by the rectangular prism chip while the screw feeder is considered as a cylinder. Because this assumption does not account for the flights of the screw, the predicted biomass temperatures are underestimated as the thermal effect from the sides of the flight are not included. Furthermore, the model considers the system as a steady state heat transfer problem, where the biomass does not move from section to section on the screw. Therefore, in this respect, the model will overestimate the temperature of the biomass. The optimal residence time for this model was calculated based on the operating parameters shown in Table 3. Assuming perfect conditions, it was found that a single particle of biomass takes approximately 7.2 seconds to travel from inlet to outlet,

staying approximately 0.6 seconds in each section of the screw. From this result, for such a large temperature gradient (500˚C to 25˚C), it is highly unlikely that there would be complete transfer of energy from the screw to the biomass. However, there will still be an effect from conduction on the overall heat transfer in the form of transient conduction where there is partial transfer of energy based on time. The conditions for transient conduction are much more sophisticated and difficult to model accurately. Therefore, radiation is the dominant form of heat transfer in this system.

Table 3. Current screw feeder operating parameters

	Operating Parameters	
Input	Length (in)	12
	Pitch (in)	1
	Outer diameter (in)	3/8
	RPM	100
	Surface Roughness factor	0.1
	Friction coeff	0.3
Output	Ideal Residence Time (s)	7.2
	Residence Time/ sect (s)	0.6

However, in consideration of these assumptions, the purpose of the model is to develop an understanding of the thermodynamics during high temperature feeding and obtain a rough estimate on biomass temperatures at various locations on the screw. This model will lay the foundation for future research to build on and refine these predictions.

4.4.2 Approach

A thermal model was developed in Excel to determine the radial temperature profile of the biomass, taking account of the dimensions and properties of both the screw feeder and biomass. Mechanical properties such as elastic modulus and Poisson's ratio are used in the Hertzian contact calculations. Thermodynamic properties such as emissivity and specific heat are used to calculate the temperature of the biomass due to heat transfer. The dimensions of the biomass chip were taken as 0.4 mm in length and 0.3 mm in both width and thickness. The values used in the calculations for the model are presented in Tables 4 and 5. Calculations were done based on the motor operating at a maximum torque output of 36 in-lb. The three cases considered were 100%, 50%, and 10% of the motor torque. The two values that were assumed are surface roughness and friction coefficient, as these could not be measured. Surface roughness factor was taken as 0.1 for metal on metal contacts. However, when two biomass layers are in contact, this factor is reduced to 0.01. A friction coefficient of 0.3 was also assumed when calculating the normal force experienced by the biomass from the motor torque. The critical output from these tables is the contact area half width, b, which determines the Hertzian contact area between the screw feeder and first layer of biomass.

Table 4. Biomass chip dimensions and properties

	Biomass Chip			
	Dimensions		**Properties**	
Input	Length (m)	0.0004	Therm Cond (W/mK)	0.12
	Width (m)	0.0003	E (GPa)	9
	Thickness (m)	0.0003	v	0.34
			Density (kg/m^3)	400
			Emissivity	0.84
			Cp (J/kgK)	2500
Output			Therm Resis (K/W)	20833.3
			Mass (kg)	1.44E-08

Table 5. Screw feeder dimensions and properties

	Screw feeder			
	Dimensions		**Properties**	
Input	Length (m)	0.3048	K (W/mK)	16.2
	Pitch (m)	0.0254	E (GPa)	196.5
	Outer diameter (m)	0.009525	v	0.3
	Flight height (m)	0.002	Density (kg/m^3)	8000
			Emissivity	0.4
Output	Inner diameter (m)	0.005525		

For a flight height of 2 mm, it was determined that it would require 7 layers of biomass to fill the capacity of each flight section. Figure 22 displays a schematic of the temperature at the surface of each layer of biomass, assuming surfaces in contact have the same temperature.

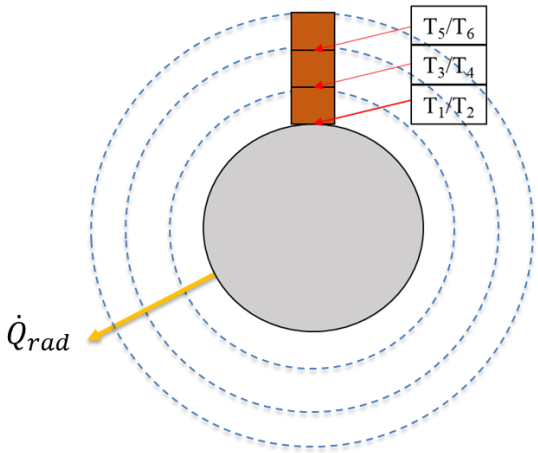

Figure 22. Schematic of first three biomass layers (brown) on screw feeder (gray)

*successive layers follow the same naming convention

The approach to determine the surface temperature of each layer of biomass is as follows. Each additional layer of biomass increases the circumference and therefore also increases the contact area. A larger contact area allows more biomass chips and results in an increase of total mass of the biomass layer. The radiative heat transfer rate was then calculated using contact area and temperature starting from the screw feeder to the top of the flight height. The temperature of the screw feeder was obtained from the thermal simulation in the previous section. From the interface, the radiative heat transfer rate is calculated outward in each layer. This value is multiplied with residence time per section to determine the total thermal energy absorbed by each biomass layer considering specific heat and mass. Using the inverse square law, the radiative heat transfer from each successive layer of biomass below and the screw feeder itself were also considered.

4.4.3 Results

Figure 23 presents an example of a plot of the calculated biomass temperature profile in the radial direction, from the interface to the top of the flight height for all 12 sections. The x-axis represents each layer of biomass and at the same time, the distance from the interface. The y-axis plots the biomass temperature. Each flight section on the screw is represented by a different colored line. The temperature profile of the biomass for all 12 sections were analyzed; however, only the first six are of interest. This is because the temperature profile in the axial direction obtained from the thermal simulation revealed that screw feeder only exceeds the combustion temperature of wood from Section 6 to the tip (Section 1). Additionally, this reduces the number of data points being presented for sake of clarity when reading the plots. These calculations are based on the current operating speed of 100 rpm, which results in a residence time of 0.6 seconds per flight.

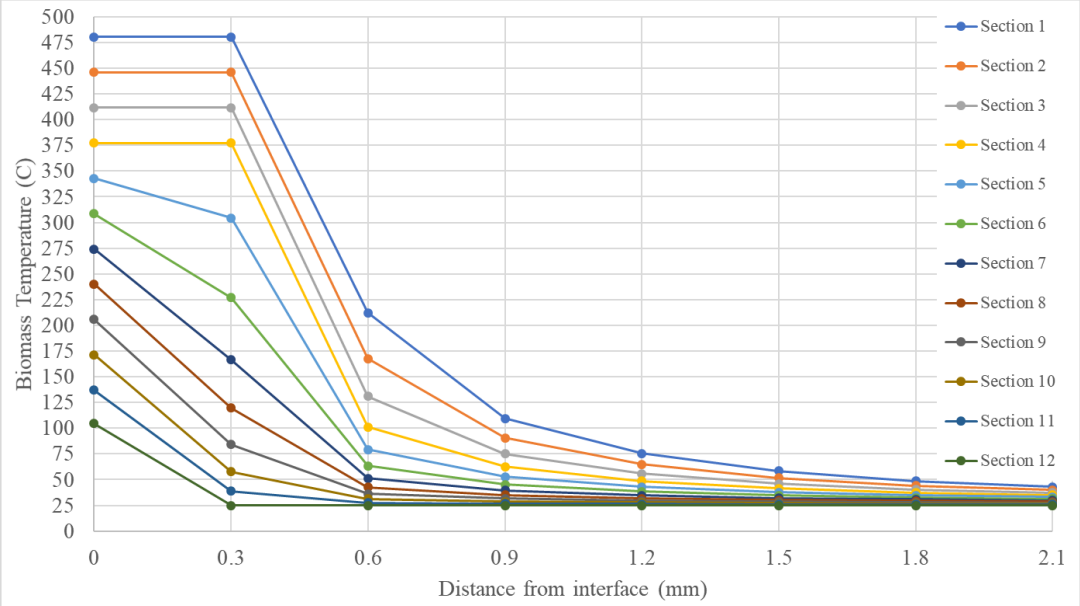

Figure 23. Sample plot of the radial biomass temperature profile for all 12 sections

For the 100% torque case, shown in Figure 24, the first layer of biomass (0.3mm in thickness) heats up to the same temperature as the screw feeder in the first four flight sections from the tip. In between the first and second layer, the biomass exceeds the ignition temperature of wood (300˚C). Section 5 will also burn at 0.3mm from the interface, but temperature dramatically decreases after this. The biomass at the contact interface of Section 6 will also burn as the screw feeder temperature is above 300˚C.

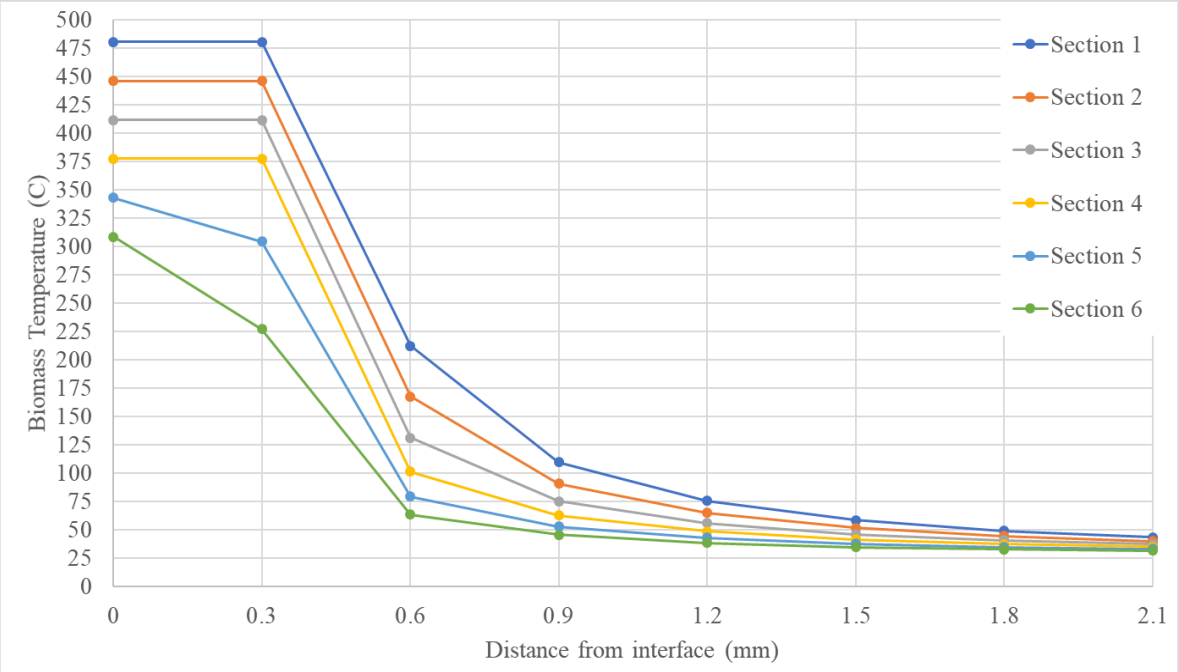

Figure 24. Radial biomass temperature profile (100% torque case)

The temperature profile for the 50% torque case, shown in Figure 25, is similar to that of the 100% case. The biomass is burned at 0.3mm from the interface at only the first four flight sections, instead of the first five. The first two section curves are the same as the 100% case, while there is a reduction in biomass temperatures for the rest of the sections.

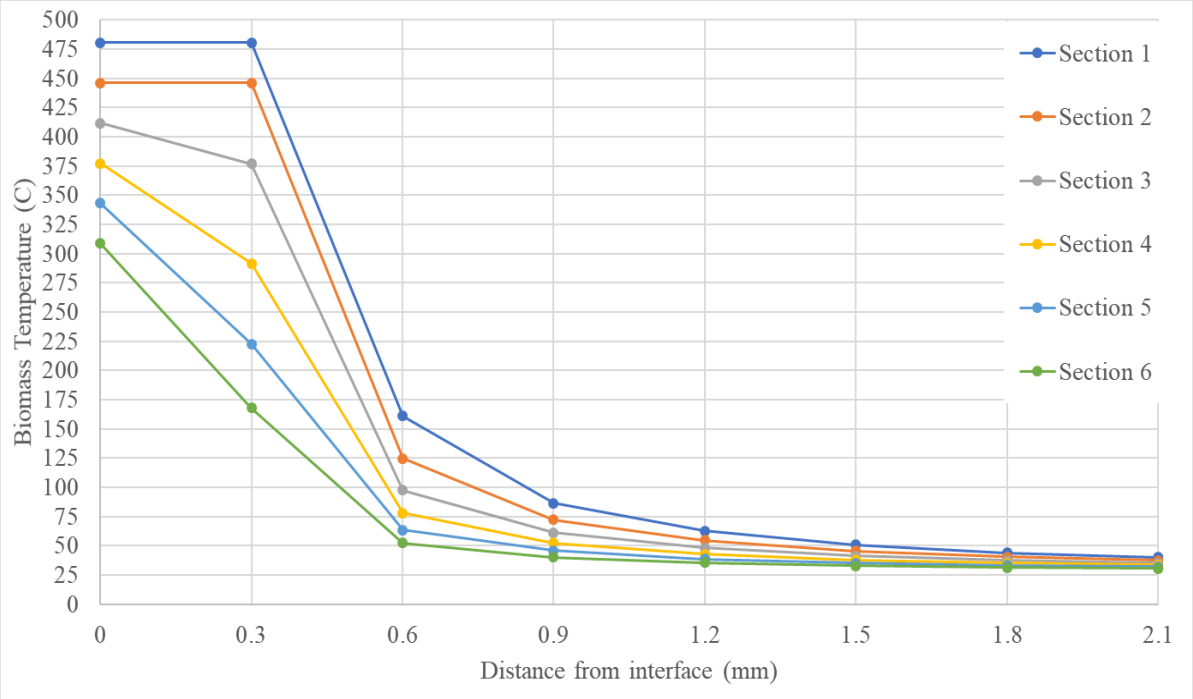

Figure 25. Radial biomass temperature profile (50% torque case)

There is a significant difference when only considering the biomass receiving 10% of the torque from the motor. As seen in Figure 26, in this case, only the biomass surface that is in contact with the screw feeder surface is burned. Note that these are assuming perfect conditions where the biomass stays in each section for only 0.6 seconds. Because of this relatively quick residence time, the temperature of the biomass at further distances from the interface decreases by a considerable amount and at a faster rate, reaching the ambient temperature sooner than the previous two cases. However, an important takeaway from this result is that the model supports the initial observations where biomass agglomeration begins to develop in Section 6 and worsens as it reaches the outlet of the screw feeder.

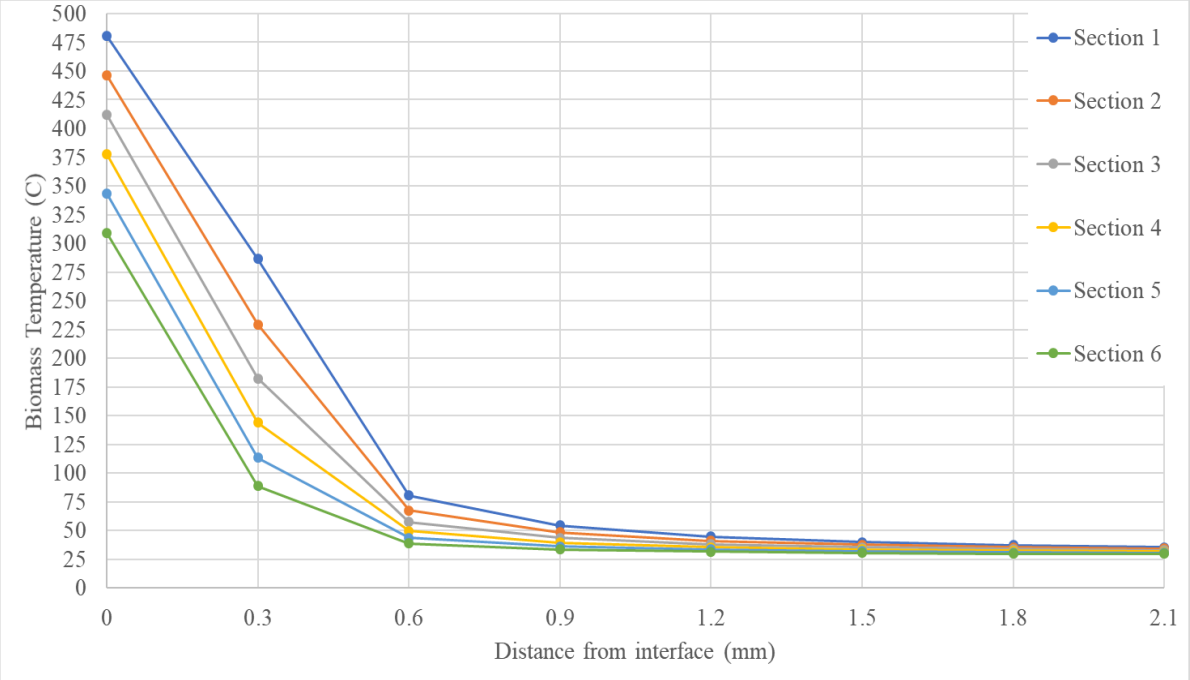

Figure 26. Radial biomass temperature profile (10% torque case)

Table 3 presents the Hertzian contact widths calculated for the three torque cases considering a biomass chip with dimensions 0.3 mm in width and thickness, and 0.4 mm in length. Notice the contact width for the 50% case and 100% case are greater than the maximum width of the biomass chip. These two cases are unlikely to occur as this means the biomass chip is smearing or deforming against the surface of the screw feeder. Furthermore, there is torque loss throughout the normal operation of the screw feeder, meaning the biomass will not be able to receive all the motor torque, which makes the 100% case impossible. Thus, the 10% case was chosen as representative of actual interface conditions and additional analysis and correlations were based on this case.

Table 3. Hertzian contact widths for varying torque cases

Motor Torque Output (in-lb)	Contact width, 2b (mm)
100%	0.704
50%	0.498
10%	0.223

4.4.4 Correlation with residence time

Using the model, it is possible to predict the thermal profile of the biomass for different lengths of residence times by adjusting the rotational speed of the screw feeder. Under realistic operating conditions, the biomass feedstock would not experience the ideal residence time due to a variety of reasons ranging from surface defects to friction. Therefore, it can be seen that for a longer residence time of 2 minutes, the following thermal profile shown in Figure 27 is obtained. A total residence time of 2 minutes would mean that the biomass particles would be present each section of the screw feeder for 10 seconds before being forced onto the next. Even in this short period of time, the biomass is burned thoroughly from the interface to the top of the flight in Sections 1-4. Based on this correlation, it can only be assumed that residence time has a positive relation to the temperature of the biomass. This means that given a long enough residence time, the biomass at all sections would reach the same temperature as the temperature of the screw feeder at the interface.

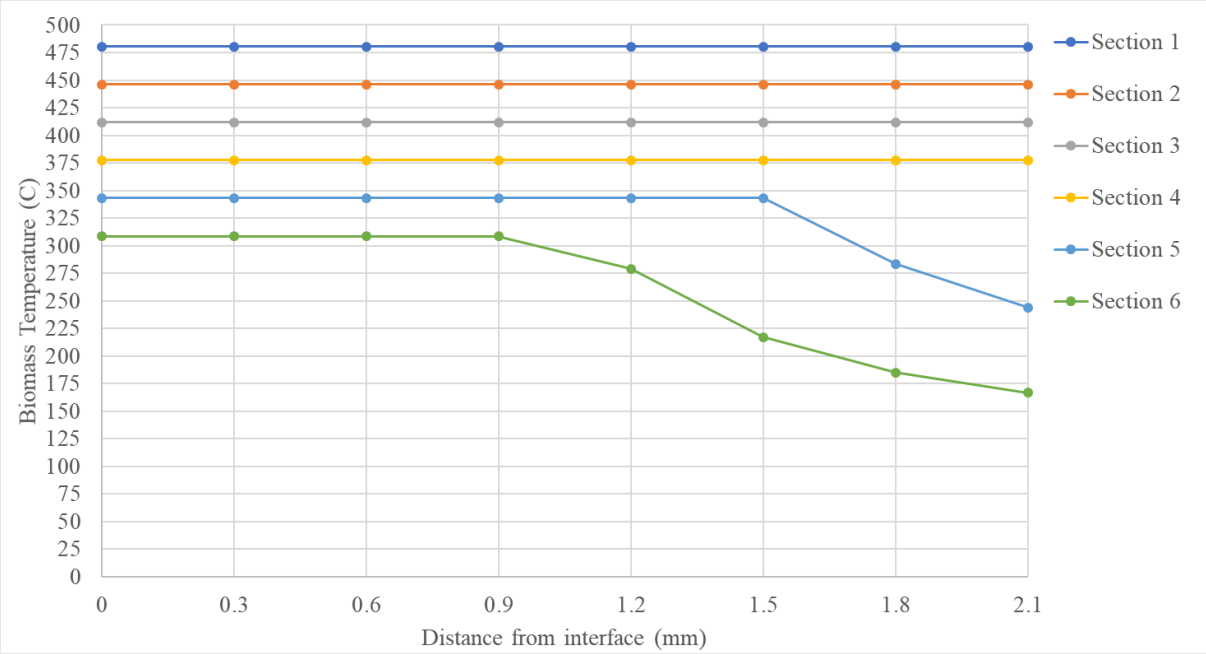

Figure 27. Biomass thermal profile when the residence time is increased to 2 minutes

In contrast, when reducing the residence time by even a factor of 0.5, there is a dramatic improvement in decreasing the temperatures experienced by the biomass in each section. This effect is clearly illustrated in Figure 28, where the total residence time was reduced to 3.6 seconds or 0.3 seconds per section. Because the residence time is shorter, the biomass moves through the screw feeder faster. Thus, there is less time for the biomass to absorb the thermal radiation energy emitted from the surface of the screw feeder and only partial heating occurs.

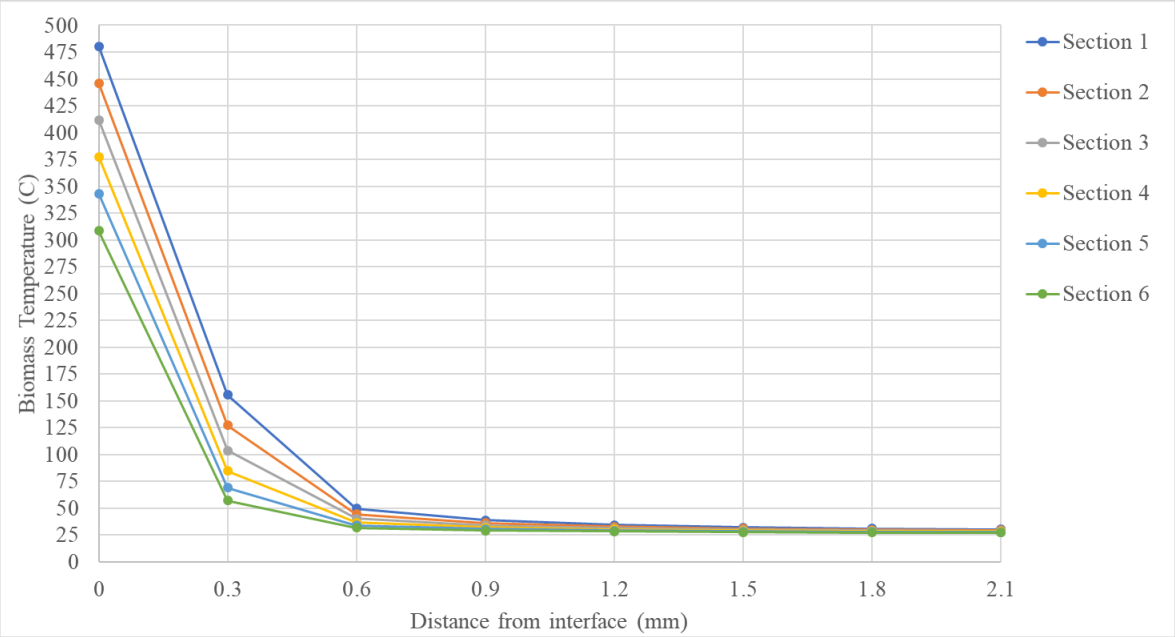

Figure 28. Biomass thermal profile when residence time is decreased to 3.6 seconds

These results show the significant effect that residence time has on the thermal profile of the biomass deposit. During high temperature feeding, residence time will play a key role in determining how much thermal energy is absorbed by the feedstock. Therefore, residence time optimization will be a critical area of improvement when developing future strategies and designs to mitigate biomass agglomeration and screw feeder plugging issues.

4.5 Summary

In this chapter, a SolidWorks model and simulation were used to obtain the axial temperature profile of the screw feeder. From this, the radial temperature profile at each section was calculated. Hertzian contact mechanics, cylinder on flat, was used to represent the contact

between the screw feeder and the biomass. Since the ideal residence time was not long enough for steady state conduction to occur, only heat transfer by radiation was considered. The radiative effect of successive layers and the screw feeder was considered using the inverse square law. The results from the thermal model present three main findings:

1. The biomass begins to burn from Section 6 to the tip.
2. There is uneven heating in each layer of biomass deposit.
3. Longer residence time results in thorough heating of the biomass deposit.

CHAPTER V

VALIDATION

This chapter covers the characterization of the biomass deposit as it travels towards the outlet of the screw feeder system. The purpose of characteration is to validate the predition of the model discussed in the previous chapter. The surface morphology and chemical composition of the biomass deposit in different sections of the screw feeder in be analyzed using a combinations of optical microscopy, SEM, and EDS. Next, the screw feeder is cross-sectionally cut in the axial direction for futher examination. Finally, correlations between the generated model and characterization results are discussed.

5.1 Biomass deposit characterization

5.1.1 Surface morphology

Characterization started in the axial direction along the screw feeder. The six flight sections selected for analysis are shown in Figure 29, where the tip is on the left and referenced as Section 1. The evolution of the biomass deposit as moves to the tip is most evident in these sections, as there are obvious changes in color and composition based on the temperature gradient.

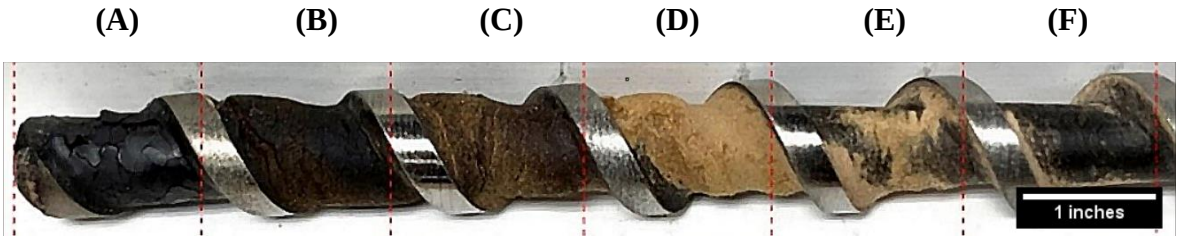

Figure 29. Nomenclature of areas chosen for analysis: (A) Section 1, (B) Section 2, (C) Section 3, (D) Section 4, (E) Section 5, (F) Section 6

Characterization began with surface morphology examination using optical microscope imaging. Figure 30 presents the optical microscope images for each section captured at x40 magnification. In Section 6, the substrate metal is covered by a thin black layer. Next, in Section 5, light-colored biomass fibers and particles begin to accumulate on the black layer. This light-colored loose fibrous deposit transitions into a darker and denser deposit as it reaches Sections 2 and 3. When arriving at Section 1, the deposit becomes black, brittle, and plate-like in structure. Based on these images, it can be seen that as the biomass reaches the tip of the screw feeder (Section 1), a change in color is observed as the deposit increased in density.

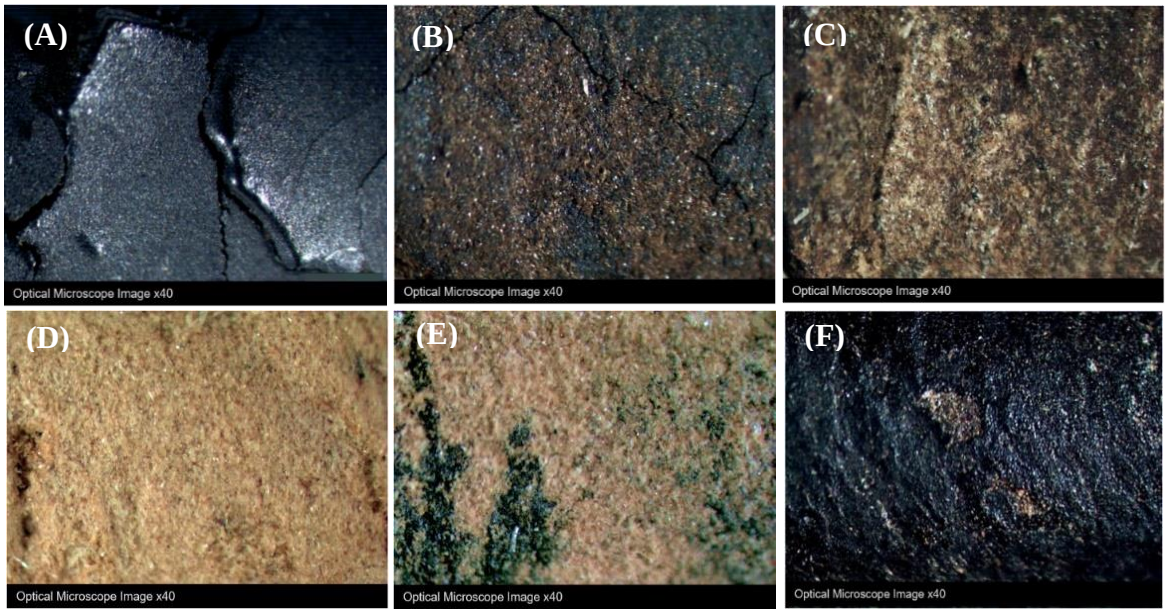

Figure 30. Optical microscope images at x40 magnification highlighting the change in appearance of the biomass deposit in (A) Section 1, (B) Section 2, (C) Section 3, (D) Section 4, (E) Section 5, (F) Section 6

Scanning electron microscopy was used to show the change in structure of the biomass. These images are shown in Figure 31 below. Starting in Section 6, the black layer that is covering the substrate appears to solid. As seen in Figure 31f, the surface is rough and uneven with evidence of brittle fractures occurring. There are also solid particles on the surface of this layer that are not representative of biomass fibers. These particles vary greatly in size and range from ~130 μm^2 to ~2500 μm^2, with an average of about 630 μm^2.

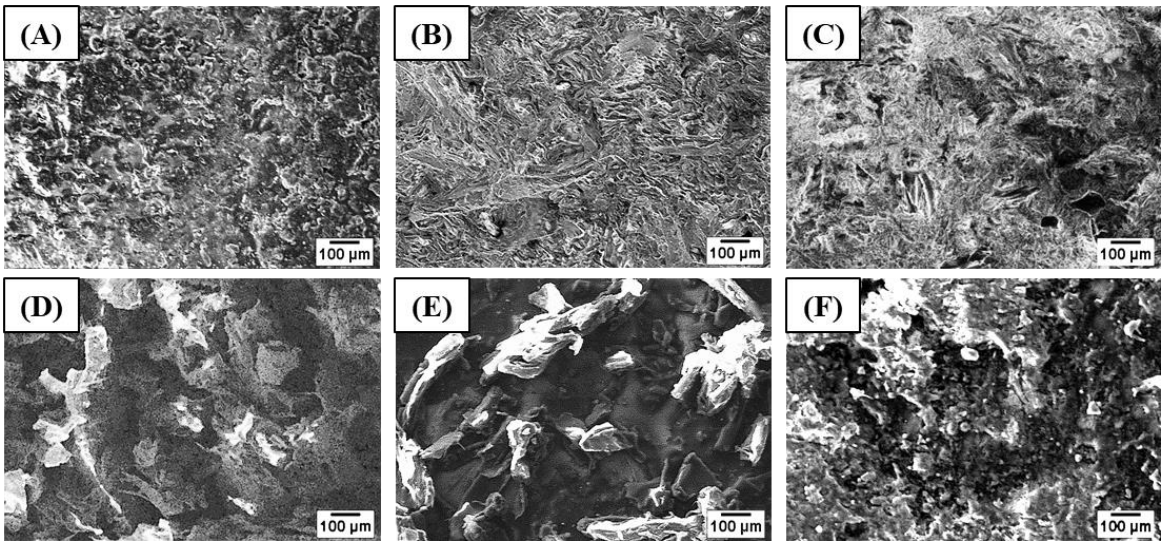

Figure 31. SEM images taken x1000 magnification revealing the evolution of biomass deposit structure (A) Section 1, (B) Section 2, (C) Section 3, (D) Section 4, (E) Section 5, (F) Section 6

In Sections 4 and 5, the SEM images, shown in Figures 31d and 31e, reveal that the deposit is similar in structure in these two sections. It is no longer solid and is composed of mostly biomass fibers. The average size of the fibers in these two sections are similar at 3700 μm^2 in Section 5 and 4000 μm^2 in Section 4. Although similar in structure, there is a significant increase in density as much more biomass fibers are present in Section 4.

Figures 31b and 31c show a distinct transformation in the biomass structure in Sections 2 and 3 on the screw feeder. Individual biomass fibers and any other particles can no longer be identified. The structure appears to be amorphous and smoother than what was observed in previous sections. This suggests that the fibers have compacted to form a denser structure.

Figure 31a reveals that the structure of the biomass deposit in Section 1 is compacted and solid. This is similar to what was observed in Section 6, however, there are no large foreign particles present. Instead, upon closer inspection, the surface seems to be embedded with much smaller particles with an average size of 220 μm^2. Overall, the surface appears to be less rough and more uniform with fewer cracks.

5.1.2 Chemical composition

EDS mapping and analysis was used to investigate the chemical composition of the biomass deposit at each flight section. Figures 32a and 32b show the distribution of carbon, oxygen, iron, and chromium on the surface of the biomass deposit in Sections 6 and 5, respectively. As expected, the biomass deposit is mainly comprised of C and O. In these two sections, the C intensity is much higher than O, indicating a greater concentration of C in the composition of the deposit. Moreover, only in these two sections are where weaker Fe and Cr signals also detected. Fe and Cr are specific to the substrate material (304SS) and do not occur in biomass. Upon further analysis of the EDS mapping for Section 6, the substrate metal can clearly be identified in an area where the surface layer fractured off. This reveals that dark layer present on the surface of Section 6 is actually a thin layer of charred biomass deposit. In Section 5, the biomass deposit begins to accumulate on top of this layer. Fe and Cr signals are significantly weaker in comparison to Section 6, however, the substrate metal can be seen in areas where there is not complete coverage by this biomass layer.

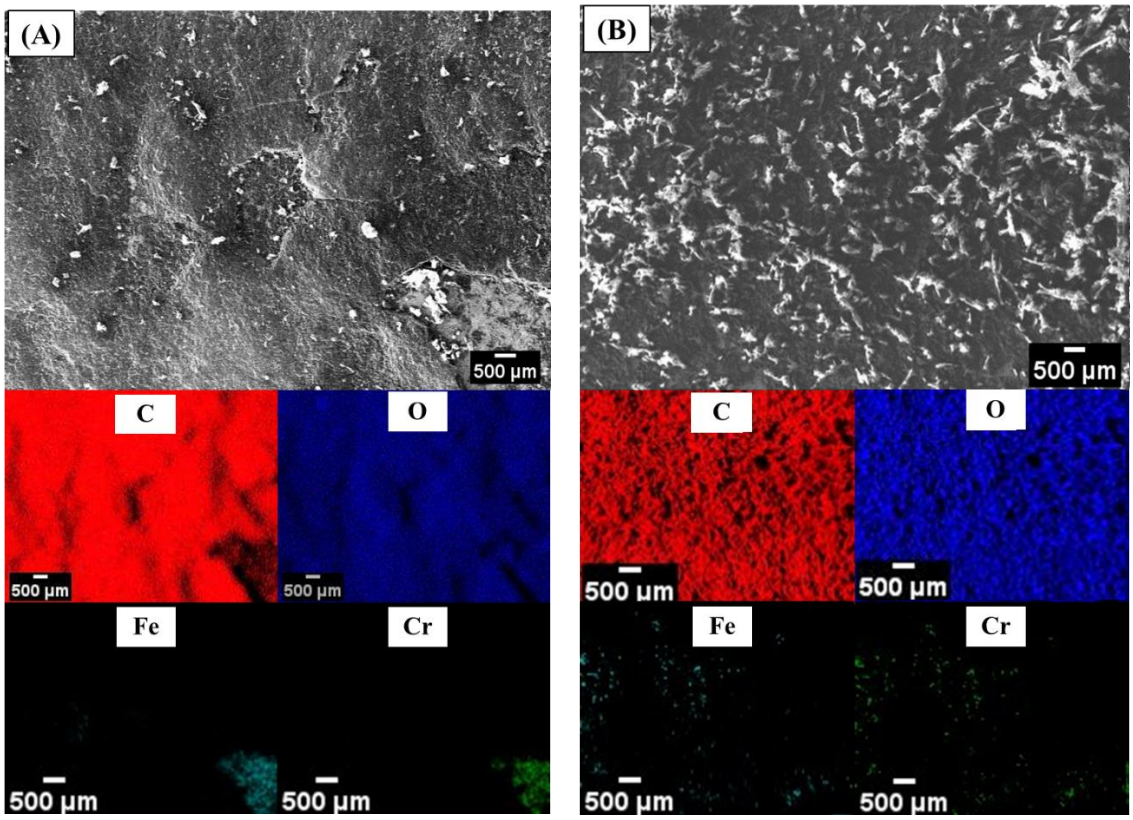

Figure 32. EDS mapping showing distribution of C, O, Fe, and Cr in (A) Section 6 and (B) Section 5

Figure 33a and 33b illustrates the change in composition of the deposit as it reaches Sections 4 and 3, respectively. Here, oxygen intensity has increased significantly relative to the previous two sections. Oxygen content reached a maximum in Section 4 then begins to decrease at Section 3. When oxygen levels are high, carbon peaks become lower, signifying an inverse relationship between C and O.

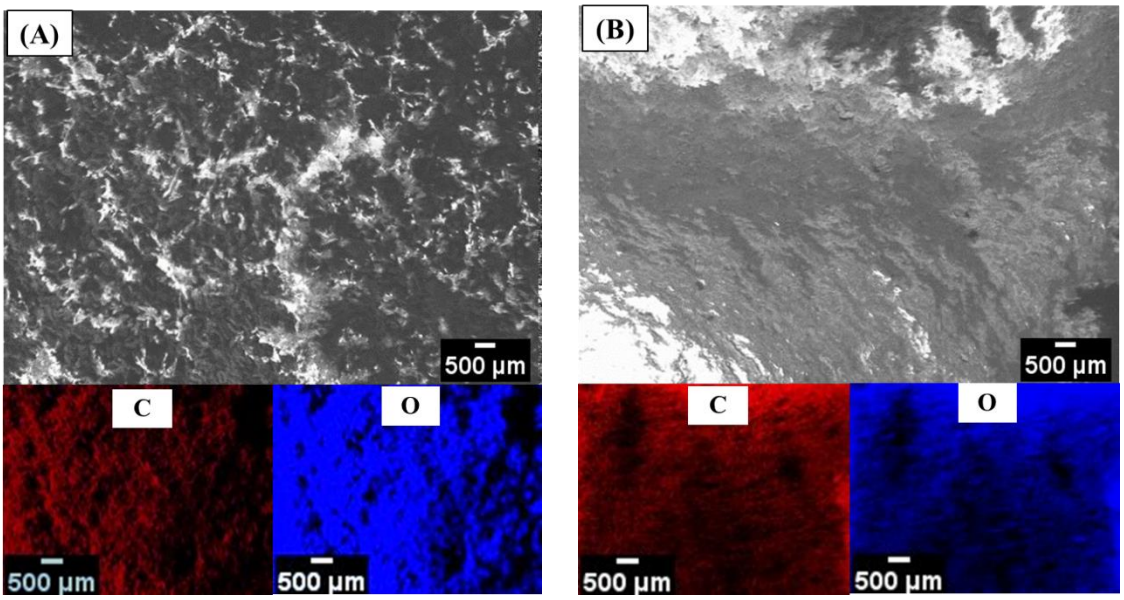

Figure 33. EDS mapping showing higher concentrations of O than C in (A) Section 4 and (B) Section 3

Figure 34 shows that the composition of the biomass deposit shifts again when reaching Sections 2 and 1. Carbon intensity increases again and reaches a maximum at Section 1. The inverse relationship is observed again as oxygen levels drop off. It is also observed that carbon levels are higher in the hardened brittle deposit as compared to other structures.

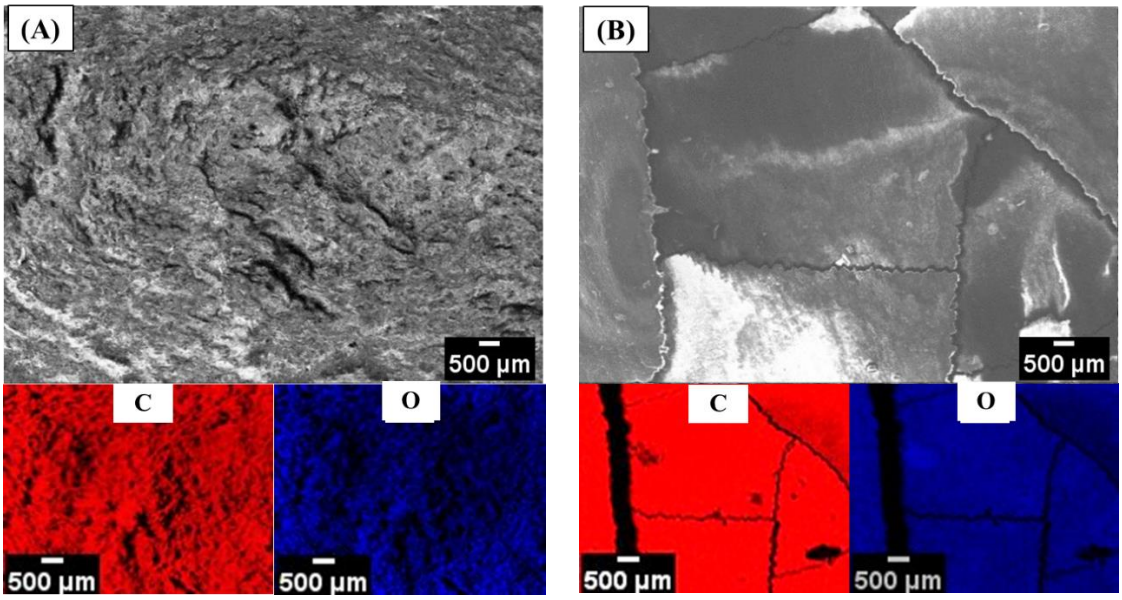

Figure 34. EDS mapping showing higher concentrations of C than O (A) Section 2 and (B) Section 1

The oxygen and carbon composition of biomass deposit at each flight section are presented in Table 6 and Figure 35. It reveals that the deposit is richer in C and poorer in O at sections where the biomass is darker in appearance and has a solid, brittle structure. This is apparent in Sections 1 and 2 where the temperatures of the screw feeder are highest. At these elevated temperatures, the biomass is heated thoroughly resulting in it being burned and decomposed into char. The deposit at Section 6 also share these same characteristics, but only a thin layer of char was formed. According to the results in the previous section, the temperature of the screw feeder at Section 6 is slightly above the combustion temperature of biomass. Thus, it is believed that only the biomass in contact with the surface of the screw feeder was burned. On the other hand, Sections 3, 4 and 5 are richer in O, meaning the biomass has not reached a temperature where it has burned yet. As seen in the optical and SEM images, individual

biomass fibers are observed and the structure of the biomass in these sections are less dense and lighter in appearance.

Table 6. Carbon and oxygen content comparison of biomass deposit at each flight section

Element	Section 1	Section 2	Section 3	Section 4	Section 5	Section 6
	Wt%	Wt%	Wt%	Wt%	Wt%	Wt%
CK	74.18	63.13	32.63	32.32	60.4	71.42
OK	22.55	28.85	50.73	59.78	33.18	19.65

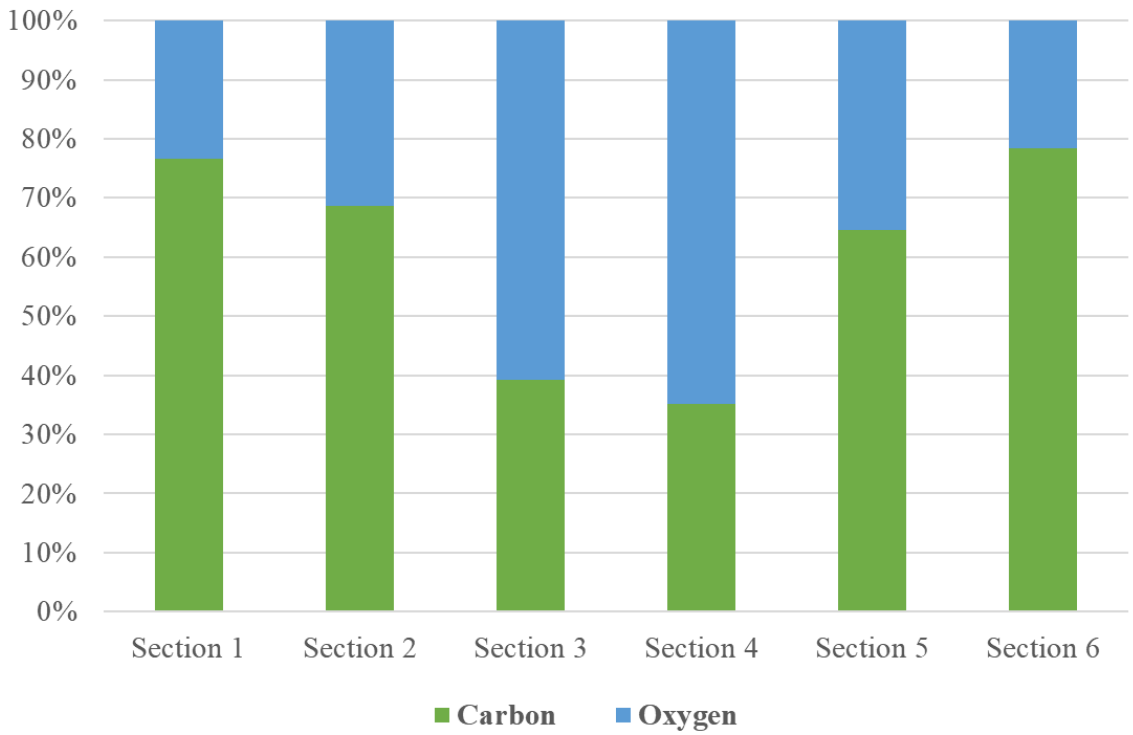

Figure 35. Carbon and oxygen comparison in each flight section

5.2 Cross-sectional examination

The screw feeder was cross sectionally cut along the axis of the screw feeder and mounted in epoxy for further analysis. The screw feeder was separated into the three samples shown in Figure 36. In these images, the white area is the screw feeder material (304SS) while the gray is biomass deposit.

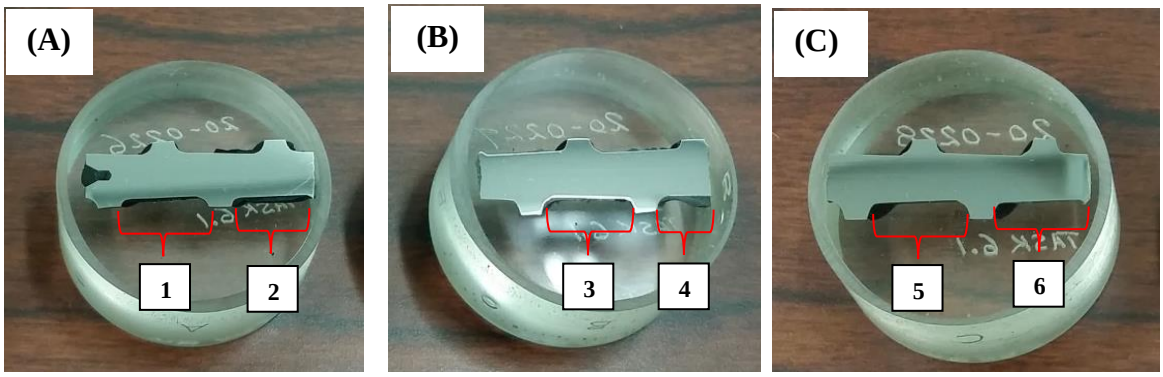

Figure 36. Epoxy mounted samples (A) tip with Sections 1 and 2 (B) Sections 3 and 4 (C) Sections 5 and 6

5.2.1 Identification of plastic deformation

Plastic deformation at the edge of the flight was discovered in Section 3. The biomass deposit here has accumulated more near the areas plastic deformation has occurred, as seen

in Figure 37. These “hooks” range from 80 to 110 μm in length and appear to be trapping additional biomass during the feeding process.

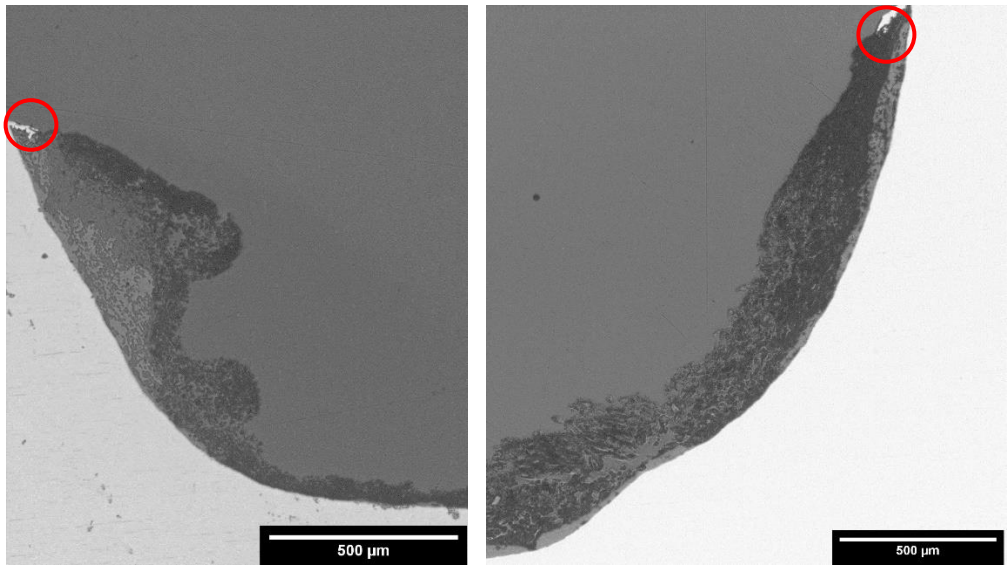

Figure 37. Optical images showing plastic deformation and biomass accumulation on both the edges of both flights in Section 3

As shown in Figure 38, the same phenomenon has occurred at the edges of the flights in Section 5. Overall, there is less biomass accumulation on the surface. However, again, where the plastic deformation has occurred, there is additional accumulation of trapped darkened biomass particles. The darker areas suggest that the biomass has been burned after being subjected to longer residence times at elevated temperatures. Here, plastic deformations are 128 to 139 μm in length are more prominent than those of Section 3.

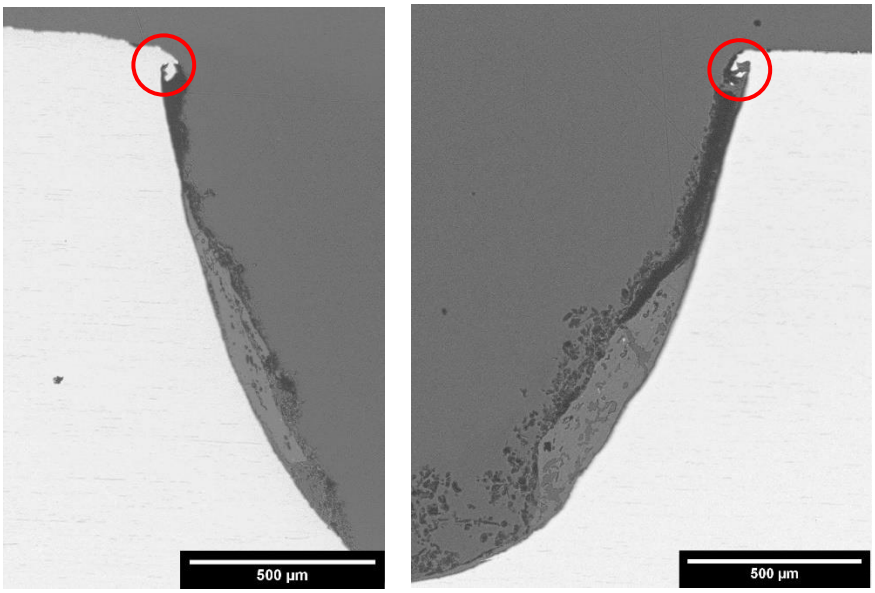

Figure 38. More severe plastic deformation and biomass accumulation on the edges of both flights in Section 5

5.2.2 Hardness

Figure 39 presents a comparison of hardness values measured by nano-indentation at Sections 1-4. Sections 5 and 6 were excluded since there was not enough biomass deposit for measurements. The deposit at Section 1 exhibited the highest hardness recorded at 0.816 GPa. The biomass hardness at Section 2 experienced a 38% reduction from Section 1 and was measured to be 0.508 GPa. The biomass deposit at Sections 3 and 4 are almost identical with hardness values of 0.390 and 0.389 GPa, respectively.

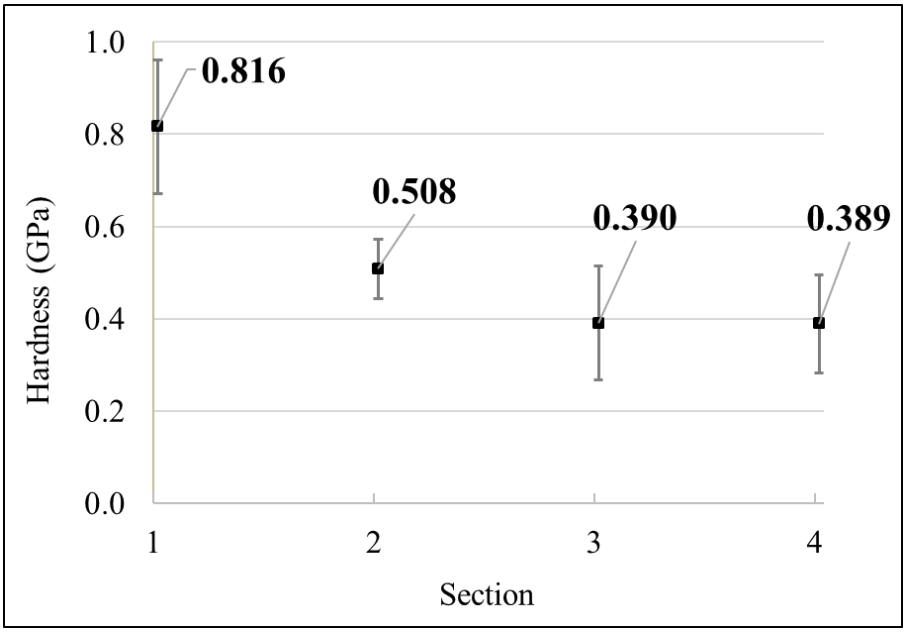

Figure 39. Biomass deposit hardness increases from Section 4 to 1

Next, hardness was measured at different areas within Section 1 and 2. The measurement areas are marked by red in Figures 40 and 41. In these images, the areas closer to the interface between the screw feeder and deposit are known as “1a” and “2a”, while the areas further from the interface are known as “1b” and “2b”.

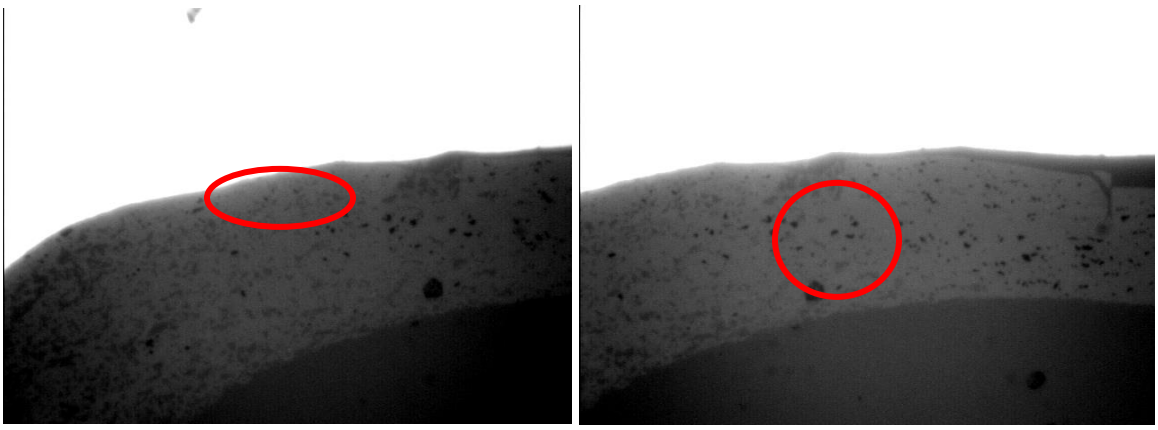

Figure 40. Nano-indentation locations in Section 1: (a) Section 1a, (b) Section 1b

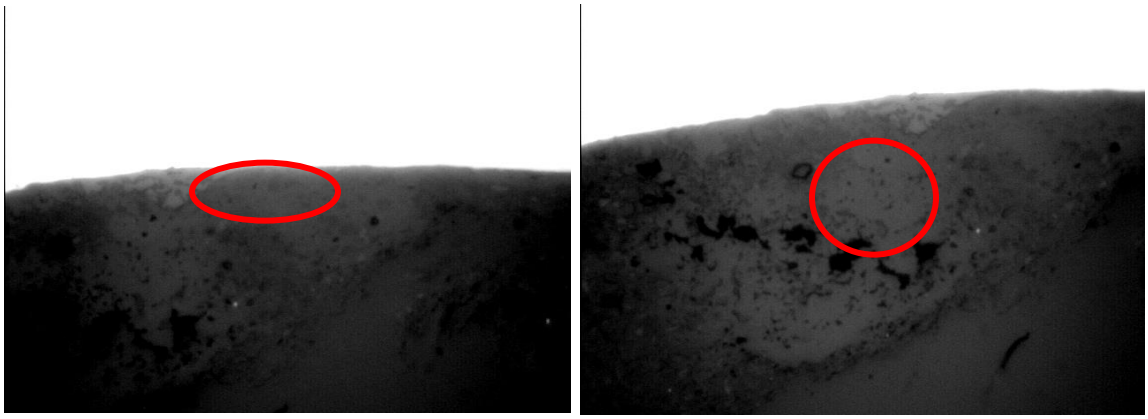

Figure 41. Nano-indentation locations in Section 2: (a) Section 2a, (b) Section 2b

Additionally, shown in Figure 42, nano-indentation was performed on an area along the interface in Section 6. This area was chosen because there was no light-colored fibrous biomass accumulation on the surface and the edge could be easily identified.

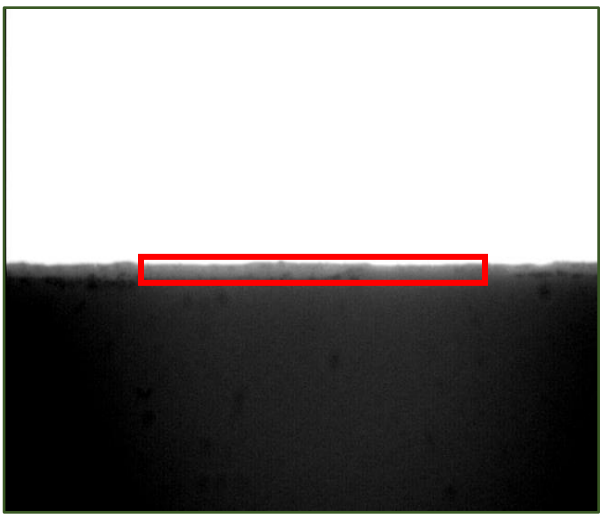

Figure 42. Nano-indentation location in Section 6

A comparison of all these hardness values with the screw material is shown in Figure 43. The biomass deposit exhibits slightly higher hardness in areas closer to the contact interface. Section 1b had a measured hardness of 0.816 GPa and experienced a 6.4% increase to 0.868 GPa at Section 1a. The hardness at Section 2b was recorded to be 0.508 GPa and saw a 24.6% increase to 0.633 GPa at Section 2a. The hardness measured at the interface of Section 6 was found to be 4.232 GPa, which is greater than the hardness of the screw material, 3.954 GPa.

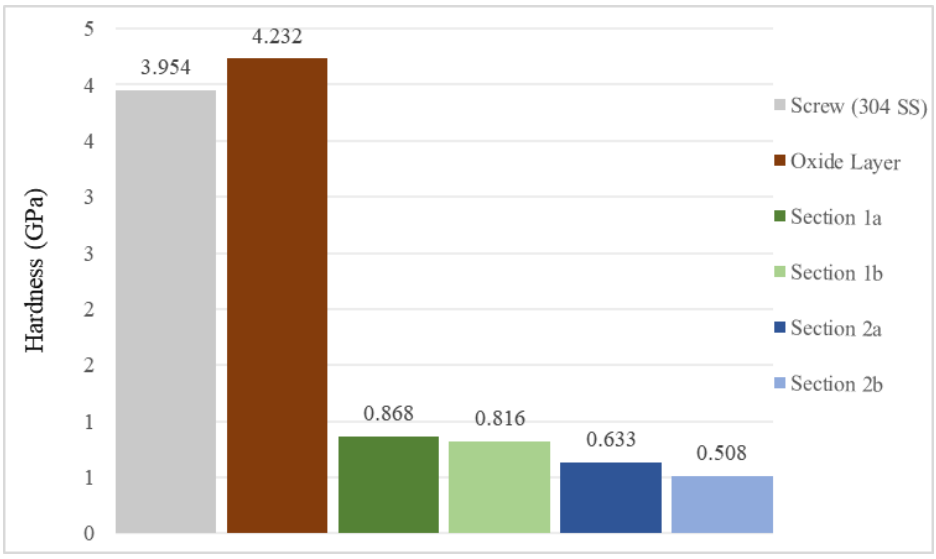

Figure 44. Hardness values are high with proximity to the interface

The hardness results show that the biomass deposit increases in hardness in each flight section as the biomass flows to the tip of the screw feeder, reaching a maximum value of 0.868 GPa at Section 1. It was also found that hardness values increase with proximity to the interface. The difference in hardness at Sections 2a and 2b show that the structure of the biomass deposit varies from the outer layer to the interface. The hardness measured at the interface of Section 6 is greater than the hardness of the screw feeder material, which suggest the presence of an oxide layer.

5.3 Summary

This chapter discussed the results obtained through characterization and their correlation with the model. Optical microscopy and SEM images reveal that the biomass deposit

changes both in appearance and structure in each section of the screw feeder. EDS analysis showed an inverse relationship between C and O. Deposits that are richer in C are darker and have more solid, brittle structures. These deposits are assumed to be burned and turned into char due to higher temperatures. The accumulation of biomass is correlated to the presence of a thin layer of charred biomass found in Section 6. This supports the findings made by the model where the temperature at Section 6 is slightly higher than the ignition temperature of biomass. The model also predicted that the biomass would be heat more thoroughly with longer residence times. This was supported by the cross-sectional examination which revealed plastic deformation at the edges of the flights that could trap additional biomass particles, thus, prolonging residence times. Furthermore, hardness values in Section 2 varied within the deposit. Higher hardness was recorded closer to the interface. This corresponds to the model's prediction that there is uneven heating of the biomass deposit with increasing distance from the interface.

CHAPTER VI

CONCLUSION AND FUTURE WORK

6.1 Conclusions

In this research, a thermal model was developed to analyze the temperature profiles of the biomass deposit and screw feeder. The axial thermal profile along the screw was found using a SolidWorks model and thermal simulations. From this, the radial temperature profile at different sections were determined using radiative heat transfer principles. Next, characterization was performed. The results from the characterization methods were then used to validate the predictions made by the model. The main findings are discussed below:

1. The results from the model show that the screw feeder exceeds the ignition temperature of wood at around Section 6. This is supported by the characterization results where there is a thin layer of charred and burned biomass covering the surface of the screw feeder.

2. The biomass that accumulates on top of the thin charred layer is initially not burned. The deposit increases in amount burned as it is exposed to higher temperature, closer to the tip of the screw feeder. This was revealed by the EDS results, where carbon and oxygen content are correlated with the severity of the burn. Higher C and lower O signifies the deposit has burned and developed char.

3. The model also showed that there is uneven heating of the biomass deposit according to the section it is in on the screw feeder. This was also supported by the change in morphology, chemical composition, and hardness of the deposit at various locations on the screw feeder.

4. It was found that residence time has a significant effect on the heating of the biomass deposit from the screw feeder. Cross-sectional examination revealed plastic deformation occurring on the edges of some flights, trapping additional biomass particles. This leads to increase residence time and accelerates biomass thermal decomposition.

The findings from this study will be beneficial to future designs for screw feeders to mitigate plugging issues. This information on biomass behavior during high temperature feeding will be valuable to the biomass feedstock industry to improve efficiency in conversion processes.

6.2 Future work

1. Strategies to mitigate biomass agglomeration and plugging should focus on reducing the residence time of the biomass feedstock during feeding. This can be done through research in material and coating selection.

2. Due to COVID 19-related delays in testing and downtime in equipment, assumptions had to be made where various properties could be tested for or measured. The model

can be improved further to account for these properties and operating parameters for more accurate analyses and predictions.

REFERENCES

[1] Bulkowska, K., Gusiatin, Z. M., Klimiuk, E., Pawłowski, A., & Pokoj, T. (2016). *Biomass for biofuels.* CRC Press.

[2] Balat, M. (2006). Biomass Energy and Biochemical Conversion Processing for Fuels and Chemicals. *Energy Sources, Part A: Recovery, Utilization, and Environmental Effects*, *28*(6), 517–525. https://doi.org/10.1080/009083190927994

[3] Jose, S., & Bhaskar, T. (2018). *Biomass and biofuels: advanced biorefineries for sustainable production and distribution*. CRC Press - Taylor & Francis Group.

[4] Gołuchowska, B., Sławiński, J., & Markowski, G. (2015). Biomass Utilization As A Renevable Energy Source In Polish Power Industry – Current Status And Perspectives. *Journal of Ecological Engineering*, *16*, 143–154. https://doi.org/10.12911/22998993/2948

[5] Shi, Y. (2013). *Biomass: to win the future*. Lexington Books.

[6] U.S. Energy Information Administration. (2020). *Biomass explained*. U.S. Energy Information Administration (EIA). https://www.eia.gov/energyexplained/biomass/.

[7] Bracmort, K. (2011). *Biomass Feedstocks for Biopower: Background and Selected Issues* . DIANE Publishing Company.

[8] Biomass Research and Development Board . (2008). Review of *The Economics of Biomass Feedstocks in the United States A Review of the Literature* . *biomassboard.gov*. Retrieved from https://biomassboard.gov/pdfs/feedstocks_literature_review.pdf

[9] Williams, C. L., Westover, T. L., Emerson, R. M., Tumuluru, J. S., & Li, C. (2015). Sources of Biomass Feedstock Variability and the Potential Impact on Biofuels

Production. *BioEnergy Research*, *9*(1), 1–14. https://doi.org/10.1007/s12155-015-9694-y

[10] Kimes , L. (2007). (rep.). *Biomass Conversion: Emerging Technologies, Feedstocks, and Products* (pp. 1–30). Washington, D.C.: U.S. Environmental Protection Agency .

[11] U.S. Energy Information Administration. (2020). *Monthly Energy Review April 2020- Table 1.3 and 10.1*. U.S. Energy Information Administration (EIA).

[12] U.S. Energy Information Administration. (2020). *Monthly Energy Review July 2020.* U.S. Energy Information Administration (EIA).

[13] U.S. Energy Information Administration. (2020). *Annual Energy Outlook 2020*. U.S. Energy Information Administration (EIA). https://www.eia.gov/outlooks/aeo/.

[14] U.S. Energy Information Administration. (2020). *Renewable Energy Consumption.* U.S. Energy Information Administration (EIA).

[15] U.S. Energy Information Administration. (2020). *Monthly Energy Review*. U.S. Energy Information Administration (EIA).

[16] National Economic Council. (2006). *Advanced Energy Initiative.*

[17] Perlack, R. D. (2005). Biomass as Feedstock for a Bioenergy and Bioproducts Industry: The Technical Feasability of a Billion-Ton Annual Supply. https://doi.org/10.2172/885984

[18] Mills, D. (2004). *Pneumatic conveying design guide* (2nd ed.). Elsevier.

[19] Metcalf, J. R. (1965). The Mechanics of the Screw Feeder. *Proceedings of the Institution of Mechanical Engineers*, *180*(1), 131–146. https://doi.org/10.1243/pime_proc_1965_180_015_02

[20] Yu, Y., & Arnold, P. (1997). Theoretical modelling of torque requirements for single screw feeders. *Powder Technology, 93*(2), 151–162. https://doi.org/10.1016/s0032-5910(97)03265-8

[21] Huo, C., Fan, C., Feng, P., Lin, W., & Song, W. (2015). Residence Time Distribution of Particles in a Screw Feeder: Experimental and Modelling Study. *The Canadian Journal of Chemical Engineering*, *93*(9), 1635–1642. https://doi.org/10.1002/cjce.22240

[22] Owen, P., & Cleary, P. (2009). Prediction of screw conveyor performance using the Discrete Element Method (DEM). *Powder Technology, 193*(3), 274–288. https://doi.org/10.1016/j.powtec.2009.03.012

[23] Wang, Y., Li, T., Muzzio, F. J., & Glasser, B. J. (2017). Predicting feeder performance based on material flow properties. *Powder Technology, 308,* 135–148. https://doi.org/10.1016/j.powtec.2016.12.010

[24] Burkhardt, G. J. (1967). Effect of Pitch, Radial Clearance, Hopper Exposure and Head on Performance of Screw Feeders. *Transactions of the ASAE, 10*(5), 0685–0690. https://doi.org/10.13031/2013.39761

[25] Carleton, A. J., Miles, J. E. P., & Valentin, F. H. H. (1969). A Study of Factors Affecting the Performance of Screw Conveyers and Feeders. *Journal of Engineering for Industry, 91*(2), 329–333. https://doi.org/10.1115/1.3591565

[26] Bates, L. (1969). Entrainment Patterns of Screw Hopper Dischargers. *Journal of Engineering for Industry*, *91*(2), 295–302. https://doi.org/10.1115/1.3591561

[27] Dai, J., Cui, H., & Grace, J. R. (2012). Biomass feeding for thermochemical reactors. *Progress in Energy and Combustion Science*, *38*(5), 716–736. https://doi.org/10.1016/j.pecs.2012.04.002

[28] Campuzano, F., Brown, R. C., & Martínez, J. D. (2019). Auger reactors for pyrolysis of biomass and wastes. *Renewable and Sustainable Energy Reviews*, *102*, 372–409. https://doi.org/10.1016/j.rser.2018.12.014

[29] Sattari-Far, I. (2003). Failure study of connecting shafts of a plug screw feeder in a paper production plant. *Engineering Failure Analysis*, *10*(3), 341–349. https://doi.org/10.1016/s1350-6307(02)00048-1

[30] Ou, L., Kim, H., Kelley, S., & Park, S. (2018). Impacts of feedstock properties on the process economics of fast-pyrolysis biorefineries. Biofuels, Bioproducts and Biorefining, 12(3), 442–452. https://doi.org/10.1002/bbb.1860

[31] Carpenter, D., Westover, T. L., Czernik, S., & Jablonski, W. (2014). Biomass feedstocks for renewable fuel production: a review of the impacts of feedstock and pretreatment on the yield and product distribution of fast pyrolysis bio-oils and vapors. *Green Chem.*, *16*(2), 384–406. https://doi.org/10.1039/c3gc41631c

[32] Lester, E., Avila, C., Pang, C. H., Williams, O., Perkins, J., Gaddipatti, S., … Wu, T. (2018). A proposed biomass char classification system. *Fuel*, *232*, 845–854. https://doi.org/10.1016/j.fuel.2018.05.153

[33] Guizani, C., Jeguirim, M., Valin, S., Limousy, L., & Salvador, S. (2017). Biomass Chars: The Effects of Pyrolysis Conditions on Their Morphology, Structure, Chemical Properties and Reactivity. *Energies*, *10*(6), 796. https://doi.org/10.3390/en10060796

[34] Li, X., Guo, X., Wang, S., Wang, K., Luo, Z., & Wang, Q. (2010). Characterization and Analysis of Char Produced by Biomass Fast Pyrolysis. *2010 Asia-Pacific Power and Energy Engineering Conference*. https://doi.org/10.1109/appeec.2010.5448524

[35] Hernández, J. J., Lapuerta, M., & Monedero, E. (2016). Characterisation of residual char from biomass gasification: effect of the gasifier operating conditions. *Journal of Cleaner Production*, *138*, 83–93. https://doi.org/10.1016/j.jclepro.2016.05.120

[36] Kuba, M., Fürsatz, K., Janisch, D., Aziaba, K., Chlebda, D., Łojewska, J., … Hofbauer, H. (2020). Surface characterization of ash-layered olivine from fluidized bed biomass gasification. *Biomass Conversion and Biorefinery*. https://doi.org/10.1007/s13399-020-00863-2

[37] Avila, C., Pang, C. H., Wu, T., & Lester, E. (2011). Morphology and reactivity characteristics of char biomass particles. *Bioresource Technology*, *102*(8), 5237–5243. https://doi.org/10.1016/j.biortech.2011.01.071

[38] Grams, J., Ruppert, A., Rzeźnicka, I., Niewiadomski, M., & Jędrzejczyk, M. (2014). Surface characterization of lignocellulosic biomass submitted to pyrolysis. *Surface and Interface Analysis*, *46*(10-11), 837–841. https://doi.org/10.1002/sia.5434

[39] Trivedi, N. S., Mandavgane, S. A., & Chaurasia, A. (2017). Characterization and valorization of biomass char: a comparison with biomass ash. *Environmental Science and Pollution Research*, *25*(4), 3458–3467. https://doi.org/10.1007/s11356-017-0689-4

[40] Haas, T. J., Nimlos, M. R., & Donohoe, B. S. (2009). Real-Time and Post-reaction Microscopic Structural Analysis of Biomass Undergoing Pyrolysis. *Energy & Fuels*, *23*(7), 3810–3817. https://doi.org/10.1021/ef900201b

[41] Donohoe, B. S., Vinzant, T. B., Elander, R. T., Pallapolu, V. R., Lee, Y., Garlock, R. J., … Warner, R. E. (2011). Surface and ultrastructural characterization of raw and pretreated switchgrass. *Bioresource Technology*, *102*(24), 11097–11104. https://doi.org/10.1016/j.biortech.2011.03.092

[42] Tolbert, A. K., Yoo, C. G., & Ragauskas, A. J. (2017). Understanding the Changes to Biomass Surface Characteristics after Ammonia and Organosolv Pretreatments by Using Time-of-Flight Secondary-Ion Mass Spectrometry (TOF-SIMS). *ChemPlusChem*, *82*(5), 686–690. https://doi.org/10.1002/cplu.201700138

[43] Mitchell, Reginald & Campbell, Paul & Ma, Liqiang & Saarenpää, Ilkka. (2005). Characterization of Coal and Biomass Conversion Behaviors in Advanced Energy Systems.

[44] Ansarifar, H., & Shams, M. (2018). Numerical simulation of hydrogen production by gasification of large biomass particles in high temperature fluidized bed reactor. *International Journal of Hydrogen Energy*, *43*(10), 5314–5330. https://doi.org/10.1016/j.ijhydene.2017.10.132

[45] Kibria, M., Sripada, P., Woo, M., & Bhattacharya, S. (2019). Fate of a biomass particle during CO2 gasification: A mathematical model under entrained flow condition at high temperature. *Energy*, *168*, 1045–1062. https://doi.org/10.1016/j.energy.2018.11.155

[46] Kibria, M., Sripada, P., & Bhattacharya, S. (2020). Steady state kinetic model for entrained flow CO gasification of biomass at high temperature. *Energy*, *196*, 117073. https://doi.org/10.1016/j.energy.2020.117073

[47] Ciesielski, P. N., Crowley, M. F., Nimlos, M. R., Sanders, A. W., Wiggins, G. M., Robichaud, D., … Foust, T. D. (2014). Biomass Particle Models with Realistic Morphology and Resolved Microstructure for Simulations of Intraparticle Transport Phenomena. *Energy & Fuels*, *29*(1), 242–254. https://doi.org/10.1021/ef502204v

[48] Li, J., Paul, M. C., Younger, P. L., Watson, I., Hossain, M., & Welch, S. (2015). Characterization of biomass combustion at high temperatures based on an upgraded single particle model. *Applied Energy*, *156*, 749–755. https://doi.org/10.1016/j.apenergy.2015.04.027

[49] Riaza, J., Khatami, R., Levendis, Y. A., Álvarez, L., Gil, M. V., Pevida, C., … Pis, J. J. (2014). Combustion of single biomass particles in air and in oxy-fuel conditions. *Biomass and Bioenergy*, *64*, 162–174. https://doi.org/10.1016/j.biombioe.2014.03.018

[50] Elmaz, F., Yücel, Ö., & Mutlu, A. Y. (2020). Predictive modeling of biomass gasification with machine learning-based regression methods. *Energy*, *191*, 116541. https://doi.org/10.1016/j.energy.2019.116541

[51] Klinger, J., Carpenter, D. L., Thompson, V. S., Yancey, N., Emerson, R. M., Gaston, K. R., … Kutnyakov, I. (2020). Pilot Plant Reliability Metrics for Grinding and Fast Pyrolysis of Woody Residues. ACS Sustainable Chemistry & Engineering, 8(7), 2793–2805. https://doi.org/10.1021/acssuschemeng.9b06718

[52] Popov, V. L. (2018). Contact Mechanics and Friction: Physical Principles and Applications. Springer.

[53] Budynas, R. G., Nisbett, J. K., & Shigley, J. E. (2020). Shigley's mechanical engineering design. McGraw-Hill Education.

[54] Budynas, R. G., Nisbett, J. K., & Shigley, J. E. (2020). Shigley's mechanical engineering design. McGraw-Hill Education.

[55] Çengel Yunus A., Boles, M. A., & Kanoglu, M. (2020). Thermodynamics: an engineering approach. McGraw-Hill Education.

[56] Askeland, D. R., Fulay, P. P., & Wright, W. J. (2011). The science and engineering of materials. Cengage Learning.

[57] Bozkurt, Görkem & Atasoy, Ilke & Boşdurmaz, Ekin Bircan. (2019). Thermal Radiation: Introduction to Thermal Radiation & Inverse Square Law. 10.13140/RG.2.2.11280.66561.

[58] Engineering ToolBox. (2003). Fuels and Chemicals - Autoignition Temperatures. Engineering ToolBox. https://www.engineeringtoolbox.com/fuels-ignition-temperatures-d_171.html.

APPENDIX

Table A1. Contact area and total mass calculations for 10% case

Layer	Thickness(m)	Circum (m)	# chips	Contact Width (m)	Contact Area/Sect	Total mass (kg)
0	0	0.0174	57.86	0.0127	0.000322	8.21E-07
1	0.0003	0.0192	64.14	0.0192	0.000488	9.22E-07
2	0.0006	0.0211	70.42	0.0210	0.000533	1.01E-06
3	0.0009	0.0230	76.71	0.0228	0.000579	1.09E-06
4	0.0012	0.0249	82.99	0.0246	0.000625	1.18E-06
5	0.0015	0.0268	89.27	0.0267	0.000678	1.28E-06
6	0.0018	0.0287	95.56	0.0285	0.000724	1.37E-06

Table A2. Thermal calculations for 10% case

	Layer 1	0.3 mm	(hertzian:s-b)	Layer 2	0.6 mm	(b-b)	Layer 3	0.9 mm	(b-b)
Sec #	Qdot (W)	Q (J)	dT	Qdot (W)	Q (J)	dT	Qdot (W)	Q (J)	dT
1	0.235	0.141	68.846	0.064	0.039	16.742	0.031	0.018	7.336
2	0.195	0.117	57.124	0.049	0.030	12.826	0.025	0.015	5.946
3	0.161	0.096	46.966	0.038	0.023	9.980	0.020	0.012	4.851
4	0.131	0.078	38.232	0.030	0.018	7.838	0.017	0.010	3.971
5	0.105	0.063	30.771	0.024	0.014	6.182	0.014	0.008	3.255
6	0.084	0.050	24.460	0.019	0.011	4.881	0.011	0.007	2.670
7	0.066	0.039	19.176	0.015	0.009	3.847	0.009	0.006	2.192
8	0.051	0.030	14.797	0.012	0.007	3.024	0.008	0.005	1.804
9	0.038	0.023	11.215	0.009	0.005	2.371	0.006	0.004	1.490
10	0.028	0.017	8.330	0.007	0.004	1.856	0.005	0.003	1.240
11	0.021	0.012	6.040	0.006	0.003	1.454	0.004	0.003	1.043
12	0.015	0.009	4.346	0.004	0.003	1.160	0.004	0.002	0.897

Layer 4	1.2 mm	(b-b)	Layer 5	1.5 mm	(b-b)	Layer 6	1.8 mm	(b-b)	Layer 7	2.1 mm	(b-b)
Qdot (W)	Q (J)	dT	Qdot (W)	Q (J)	dT	Qdot (W)	Q (J)	dT	Qdot (W)	Q (J)	dT
0.020	0.012	4.422	0.015	0.009	2.960	0.011	0.007	2.121	0.009	0.006	1.638
0.017	0.010	3.656	0.012	0.007	2.497	0.010	0.006	1.830	0.008	0.005	1.446
0.014	0.008	3.045	0.010	0.006	2.126	0.009	0.005	1.596	0.007	0.004	1.291
0.012	0.007	2.550	0.009	0.005	1.824	0.007	0.004	1.404	0.007	0.004	1.164
0.010	0.006	2.144	0.008	0.005	1.575	0.007	0.004	1.246	0.006	0.004	1.058
0.008	0.005	1.810	0.007	0.004	1.370	0.006	0.004	1.115	0.006	0.003	0.970
0.007	0.004	1.537	0.006	0.004	1.201	0.005	0.003	1.007	0.005	0.003	0.898
0.006	0.004	1.314	0.005	0.003	1.063	0.005	0.003	0.918	0.005	0.003	0.838
0.005	0.003	1.133	0.005	0.003	0.951	0.005	0.003	0.846	0.004	0.003	0.788
0.005	0.003	0.988	0.004	0.003	0.861	0.004	0.003	0.787	0.004	0.003	0.748
0.004	0.002	0.874	0.004	0.002	0.789	0.004	0.002	0.740	0.004	0.002	0.715
0.004	0.002	0.789	0.004	0.002	0.735	0.004	0.002	0.704	0.004	0.002	0.689

Table A.3. Biomass temperatures for 10% case

	Distance from interface (mm)							
	0	**0.3**	**0.6**	**0.9**	**1.2**	**1.5**	**1.8**	**2.1**
Sec#	**T1/T2 (C)**	**T3/T4 (C)**	**T5/T6 (C)**	**T7/T8 (C)**	**T9/T10 (C)**	**T11/T12 (C)**	**T13/T14 (C)**	**T15/T16 (C)**
1	480.40	286.46	80.42	54.36	44.84	39.99	37.19	35.60
2	446.05	229.33	67.59	48.41	41.18	37.50	35.36	34.16
3	411.70	182.37	57.61	43.56	38.14	35.37	33.77	32.87
4	377.37	144.14	49.77	39.59	35.59	33.55	32.36	31.70
5	343.02	113.36	43.59	36.34	33.44	31.97	31.12	30.65
6	308.66	88.90	38.71	33.67	31.63	30.60	30.00	29.67
7	274.33	69.73	34.86	31.47	30.10	29.40	29.00	28.78
8	239.98	54.93	31.84	29.67	28.78	28.34	28.08	27.94
9	205.64	43.72	29.47	28.18	27.65	27.39	27.23	27.15
10	171.34	35.39	27.61	26.94	26.66	26.52	26.44	26.40
11	137.04	29.35	26.16	25.90	25.79	25.74	25.70	25.69
12	104.64	25	25	25	25	25	25	25
	(SW)							